Younger and brighter - New distances to globular clusters based on Hipparcos parallax measurements of local subdwarfs

I. Neill Reid
Palomar Observatory, 105-24, California Institute of Technology, Pasadena, CA 91125,
e-mail: inr@astro.caltech.edu

ABSTRACT

We have used new parallax measurements, obtained by the Hipparcos satellite, of fifteen nearby, metal-poor stars to re-define the subdwarf main-sequence. All of these stars have parallaxes determined to an accuracy of at least 12 %. Comparing these measurements against previous ground-based data for nine stars reveals a systematic offset of 5 %, in the sense that the Hipparcos parallaxes are smaller (i.e. the inferred distances are larger). The availability of the Hipparcos observations expands the local subdwarf sample to the extent that we can separate the stars by abundance into intermediate ([Fe/H] $\sim$ -1.4) and extreme ([Fe/H] ~ -2) subsets. Main-sequence fitting techniques are then used to match stars of the appropriate abundance range to the colour-magnitude diagrams of the seven globular clusters M5, NGC 6752, M13, M15, M92, M30 and M68. We derive respective distance moduli of 14.45, 13.17, 14.48, 15.38, 14.93, 14.95 and 15.29 magnitudes, with formal uncertainties of $\pm$0.1 magnitude. The metal-poor systems M68, M15 and M30 have moderate foreground reddening, and varying E_{B-V} by $\pm$0.02 magnitudes can change the derived distances by up to $\pm$7%. With the exception of NGC 6752, however, our derived distances exceed previous estimates, particularly in the case of the four [Fe/H]~ -2.1 globulars, where our distance moduli are $\sim$ 0.3 magnitudes higher than the current standard values. We discuss briefly how these findings affect the RR Lyrae distance scale, isochrone-based estimates of the age of globular clusters and our picture of the early stages of star formation in the Galaxy. We note that our results go some way towards reconciling the apparent contradiction between the cluster ages and recent determinations of the Hubble constant.

Subject headings: Stars: subdwarfs, parallaxes; Globular clusters: distances

1. Introduction

Globular clusters constitute a vital rung on the extragalactic distance ladder. Not only do they provide a means of calibrating the absolute magnitudes of secondary distance indicators, such as short-period miras and RR Lyraes, but also comparisons between their colour-magnitude diagrams and the predictions of stellar evolutionary models can be used both to probe the early star-formation history of the Galaxy and to set a lower limit on the age of the universe. Both issues are controversial at present. In the first case, most isochrone-based colour-magnitude diagram analyses derive ages of from 14 to 18 Gyrs for the majority of globular clusters, (Chaboyer, Demarque & Sarajedini, 1996; Sandquist et al, 1996 - hereinafter S96). Bolte & Hogan (1995 - BH95), in particular, have argued that matching the best cluster data against theoretical isochrones leads to age estimates of 15.8±2.1 Gyrs. These timescales are in conflict with recent estimates of the expansion age of the Universe. The "mid-term" value of 73 ± 10 km s^{-1} Mpc^{-1} derived for the Hubble constant by the HST key project team (Freedman, Madore & Kennicutt, 1997) implies an age of only 9 to 12 Gyrs when interpreted in standard $\Lambda = 0$ cosmological frameworks (Freedman, priv. comm.), although the long distance-scale value of $H_0 = 50$ to 55 km s^{-1} Mpc^{-1} favoured by Tammann & Sandage (1996) is formally consistent with the stellar chronometers.

In the second case, there is a long-standing discrepancy between the distance to the Large Magellanic Cloud that one derives using the RR Lyrae absolute magnitude calibration and that computed based on the Cepheid scale. The traditional calibration of the latter period-luminosity relation, based on Galactic Cepheids, leads to an LMC distance modulus of 18.57 (Feast, 1997). A small number of the older LMC clusters with extensive RR Lyrae populations have been monitored photometrically, allowing the determination of accurate mean magnitudes. In particular, five clusters with [Fe/H]=-1.8±0.1 (from Walker, 1992 and Reid & Freedman, 1994) give a mean magnitude, corrected for foreground reddening, of $< V_0 >= 18.98 \pm 0.03$ for LMC RR Lyrae variables. If one adopts the absolute magnitude calibration given by statistical parallax analysis of the halo RR Lyraes in the Solar Neighbourhood, $< M_V >= 0.71 \pm 0.12$ mag, with little dependence on abundance (Layden et al, 1996) then one derives an LMC modulus of only 18.3 magnitudes.

Baade-Wesselink analyses of Galactic field stars, however, suggest that there is a significant correlation between luminosity and abundance, although there is as yet no clear agreement as to the exact correlation. Carney et al (1992a) derive a shallow slope of only 0.15 mag. dex^{-1} in M_V and a zeropoint of M_V=1.01 at [Fe/H]=0.0; Fernley (1994) finds a slope of 0.21 and a zeropoint of $M_V = 0.97$ mag; Cacciari, Clementini & Fernley (1992) previously estimated a similar slope of 0.2, but a fainter zeropoint, M_V=1.04; and Sandage

(1993) derives a steeper slope, 0.3 mag. dex^{-1}, and a brighter zeropoint, M_V=0.94 mag. Finally, Feast (1997) has used inverse regression to re-analyse the Fernley sample, and drives a yet-steeper slope, 0.37 mag dex^{-1}, and the faintest zeropoint, M_V=1.13. Combined with the mean observed magnitude, $< V_0 >$= 18.98 mag at [Fe/H]=-1.8, these five different calibrations lead to LMC distance moduli estimates of, respectively, 18.24, 18.39, 18.30, 18.58 and 18.52 magnitudes. The last two estimates are in acceptable agreement with the traditional Cepheid values and with the older distance estimate based on SN 1987A (Panagia et al, 1991), although Gould (1995) has recently advocated $(m\text{-}M)_0$=18.37 mag for the latter, matching the shorter distance scale. [1] However, Feast & Catchpole (1997) have recently re-calibrated the zeropoint of the Cepheid period-luminosity relationship using Hipparcos parallax estimates of Galactic variables, and now propose a true LMC modulus of 18.7 magnitudes, restoring the disagreement between the Cepheid and RR Lyrae-based distance scales.

As Sandage (1986) has emphasised, both cluster age-determinations and the calibration of the absolute magnitude of horizontal branch stars rest on the accuracy of the distances to individual globular clusters. Those distances can be estimated either empirically, by main-sequence fitting - matching the observed cluster colour-magnitude diagram against the main-sequence defined by stars of the appropriate metallicity which have accurate trigonometric parallax measurements - or in a semi-empirical fashion, matching theoretical isochrones, calibrated against the local subdwarfs, to the observed cluster sequences. The latter technique depends on the availability of accurate bolometric corrections and temperature-colour calibrations to transform from the (Luminosity, temperature) plane to the observed (M_V, colour) plane. Generally, most previous studies have agreed in deriving cluster ages of 14 or more Gyrs from either technique. A notable exception is the analysis by Mazzitelli, D'Antona and Caloi (1995), based on updated physical parameters, which lead to more luminous horizontal-branch stellar models. Coupled with a new treatment of convection, which reduces the turnoff age for a given luminosity, they derive younger ages (12-14 Gyrs) for the metal-poor clusters.

The primary observational method for deriving cluster distances is main-sequence fitting against subdwarfs of known absolute magnitude and colour. Since globular clusters are significantly more metal-poor than the Sun, the calibrating parallax stars must be drawn from the Galactic halo population, which constitutes only $\sim 0.15\%$ of the local stars. While there are a few M-type subdwarfs (such as Kapteyn's star) within 10 parsecs of the Sun, the nearest F and G subdwarfs lie at distances of 40-50 parsecs. As a result, until recently

[1]Feast & Catchpole note that Sonnenborn et al. (preprint), argue that a better estimate is 18.46 ± 0.10 mag., with possible systematic uncertainties still to be taken into account.

there were scarcely a dozen stars whose distances were known to sufficient precision to allow their use as calibrators. Those stars, moreover, span an abundance range of well over 1 dex, requiring the application of differential colour corrections (derived from theoretical isochrones) to adjust each star to an appropriate mono-metallicity sequence before matching the colour-magnitude data for an individual cluster. The required corrections can be substantial: for example, adjusting the observations of HD 23439A ([Fe/H] = -1.02) to match the Bergbusch & Vandenberg (1992 - BV92) [Fe/H]=-2.0 isochrone demands a correction of ∼-0.1 magnitudes to the (B-V) colour (cf S96, Table 9).[2] These corrections, moreover, are model dependent. D'Antona, Caloi and Mazzitelli (1997 - DCM) derive a colour-shift of $\frac{\Delta(B-V)}{\Delta[Fe/H]}$ of 0.056 mag, and, using the same small sample of calibrators as BH95, derive significantly larger distances to metal-poor clusters like M92. Finally, one should also bear in mind the fact that cluster abundances are usually measured using red giant stars, while the field subdwarfs are (obviously) unevolved.

The successful completion of the Hipparcos astrometric satellite project and the publication of the Hipparcos catalogue (ESA 1997) has improved markedly the prospects of obtaining accurate distance calibration to globular clusters. Not only has the Hipparcos team provided more accurate parallaxes for the "classical" subdwarf calibrators, but the sample of metal-poor stars has been increased to the point at which one can isolate sufficient stars within a limited range of abundance to define a main-sequence without recourse to significant colour corrections. We have obtained Hipparcos data for a sample of proper motion stars which includes fifteen subdwarfs with abundances in the range -2.2 ≥ [Fe/H] ≥ -1.25, and we have combined these observations with data for three additional stars with accurate ground-based astrometry to derive distances to seven globular clusters. In six cases, our derived distance moduli are higher than currently accepted values, particularly for the metal-poor clusters. The following section presents the new parallax data; section 3 describes the main-sequence fitting and the distance derived for each cluster; and section 4 discusses our conclusions.

2. The subdwarf calibration

The Hipparcos satellite was launched with the aim of obtaining accurate positions, parallaxes and proper motions for over 110,000 relatively bright stars distributed over

[2]Note that to be physically correct, this procedure should preserve mass - that is, both the colour and the absolute magnitude of a given subdwarf should be adjusted to those appropriate to a star of the equivalent mass at the abundance of the cluster. The M_V corrections are not usually applied in practice.

the whole sky. Despite the problems introduced by the satellite's failure to leave a highly-elliptical orbit, the separate consortia completed their data reduction in late 1996, achieving the goal of milliarcsecond-precision astrometry. The reduction procedures are discussed by Kovalevsky et al (1995), while Perryman et al (1995) describe the tests carried out to establish the accuracy of the resultant parallax measurements. Part of the Hipparcos programme consisted of observations of a substantial fraction of the Lowell proper motion stars (Giclas, Burnham & Thomas, 1971) brighter than V=12 magnitude, a proposal submitted by the author in 1982. Some 2500 stars were observed, including five "classical" subdwarfs (S96, Table 9) together with a number of other well-known subdwarfs, such as HD 19445 and HD 84937. In addition, since the inception of the Hipparcos project, many of the F, G and early-K stars in the Lowell survey have been observed spectroscopically and photometrically by Carney, Latham and Laird (Carney et al, 1994: CLLA); these observations have added several stars to the small sample of known, nearby metal-poor subdwarfs with accurate photometry and abundance estimates.

Seven hundred and forty-five of the 1447 stars in the CLLA catalogue have Hipparcos astromtery. The complete set of observations offers insight into both the detailed structure of the lower main-sequence and the kinematics of the higher velocity stars in the disk, and these matters will be discussed in detail elsewhere (Reid, in preparation). In the present paper we concentrate on the metal-poor stars. One hundred and six of the CLLA stars observed by Hipparcos have [Fe/H]<-1.25, but only thirty-five of these stars have parallaxes determined to a precision ($\frac{\sigma_\pi}{\pi}$) of 20 % or better. The relevant data for these stars are listed in Table 1, where we have divided the sample into two groups: fifteen stars with parallaxes measured to a precision of at least 12 %, which represent our primary calibrators, and 20 stars with less precise parallax data. The photometry and abundance estimates are taken directly from Table 6 of CLLA. Eleven stars are listed as having significant foreground reddening by CLLA, and we have corrected the magnitudes and colour appropriately. Six stars are found to be single-lined spectroscopic binaries by CLLA, and a further 8 stars are candidate binaries based one either radial velocity data or the Hipparcos astrometry. These stars are identified in Table 1. Twenty-six stars from the complete sample are listed in the recently-published Yale General Catalogue of Trigonometric Parallaxes (van Altena, Truen-liang Lee & Hoffleit, 1995 - hereinafter, YPC), and Table 1 lists YPC data for three "classical" subdwarfs which were not amongst our Hipparcos observations. However, before comparing these astrometric data against previous measurements, it is important to consider the appropriate method of correcting for the bias known to be present in such observations.

2.1. Systematic corrections to parallax measurements

Table 1 lists the absolute magnitudes, M_V, derived directly from the parallax data. These represent the most accurate estimate of the visual luminosity of each star. However, when combining the individual measurements in any statistical analysis, one must take into account systematic bias towards overestimating parallax measurements. Lutz & Kelker (1973 - LK) undertook the first quantitative analysis of this effect, which has the same source as Malmquist bias: if the number of stars is increasing with decreasing true parallax, π_0, then symmetric errors in the measured parallax, π, will lead a sample including more stars with overestimated parallaxes, $\pi = \pi_0 + d\pi$, than with $\pi = \pi_0 - d\pi$. That is, $\bar{\pi}_0 < \bar{\pi}$; the average distance is underestimated, and, as a consequence, the average luminosity is underestimated. Lutz and Kelker determined specific corrections for the case of a uniform stellar distribution, i.e. a parallax distribution, $P(\pi) \propto \pi^{-4}$. Smith (1987) has shown that their calculations can be described by the empirical formula

$$\Delta M_{LK} \quad = \quad 5 \times log([1 + \sqrt{1 - 19(\sigma_\pi/\pi)^2}]/2)$$

However, Hanson (1979) has demonstrated that the constant-density LK corrections are seldom appropriate for analysing observational samples, where magnitude and proper-motion limits can modify the selection effects, and he derives a more general analytic representation of the LK corrections. If the parallax distribution can be characterised as a power law, $P(\pi) \propto \pi^{-n}$, then the LK correction can be approximated as

$$\Delta M_{LK} \quad = \quad -2.17 \times [(n + \frac{1}{2})\frac{\sigma_\pi}{\pi}^2 \quad + \quad (\frac{6n^2 + 10n + 3}{4})\frac{\sigma_\pi}{\pi}^4]$$

(Hanson, 1979: equation 31). The uniform density ($n = 4$) approximation lies slightly below the original Lutz-Kelker datapoints (figure 1).

If the stellar sample under study is wholly or partially magnitude-limited, as is the case with the Hipparcos observations of the Lowell proper motion stars, then one expects an exponent $n < 4$. As figure 1 shows, a smaller value of n leads to lower predicted corrections: with fewer stars at smaller parallax, the probability of overestimating an individual parallax measurement is correspondingly reduced. The appropriate exponent to use for a given sample can be estimated empirically using the cumulative proper motion distribution of the sample of stars for which one has parallax data. If $P(\pi) \propto \pi^{-n}$, and the stellar velocity distribution does not vary significantly within the sampling volume, then $N(\mu) \propto \mu^{-n+1}$.

Hanson (1979) calculates $N(\mu)$ for the complete Lowell catalogue, and finds it consistent

with a uniform distribution. However, Hipparcos observations were effectively limited to stars with $V < 12$ magnitude (80 % of the Lowell stars in this magnitude range have parallax measurements). The cumulative proper motion distribution of the full Hipparcos sample is $N(\mu) \propto \mu^{-2.4}$ ($n = 3.4$). The stars listed in Table 1 have been selected on the basis that they have parallax measurements of higher precision, hence one might expect the inclusion of a proportionately larger fraction of the nearer stars. This is the case: the proper motion distribution of the Table 1 stars shows a slower increase in number with decreasing proper motion, best matched by $N(\mu) \propto \mu^{-1.2}$ ($n = 2.2$).

The appropriate value of the parameter n to adopt in calculating the LK absolute magnitude corrections for the Table 1 subdwarf calibrators is $n = 3.4$, since that gives an appropriate characterisation of the selection effects which defined the original parallax sample (i.e. Lowell proper motion stars with V< 11). Were one to analyse the complete dataset, the Lutz-Kelker effects would be calculated on that basis. Selecting stars with high-precision measurements from that parent sample does not change the underlying systematic bias in the sample.

The resultant Lutz-Kelker corrections amount to only -0.13 magnitudes for a star whose parallax has an uncertainty of 12 %, but rise to -0.43 magnitudes as the precision drops to 20 %. In comparison, the $n = 2$ calibration (applied by S96 to their subdwarf sample) leads to corresponding corrections of -0.08 and -0.26 magnitudes - a substantial difference for the lower precision measurements. On this basis, we have divided our sample into primary calibrators with $\frac{\sigma_\pi}{\pi} < 12\%$, which we use to estimate directly the cluster distances, and the lower precision secondary calibrators, which serve to check the derived distance moduli. Averaging over the complete sample of 15 Hipparcos and 3 YPC stars listed in Table 1, there is a systematic offset of only 0.02 magnitudes between the $n = 2$ and $n = 3.4$ ΔM_{LK} calibrations. Since we weight each star by its uncertainty in matching the fiducial cluster sequences (section 3), the derived distance moduli are affected by no more 0.01 magnitudes. It is clear from figure 1, however, that the choice of the correct exponent is of considerably greater significance if one is faced with analysing a sample including many stars with parallaxes of lower precision.

2.2. A comparison with previous ground-based parallax measurements

The subdwarfs that are employed in cluster main-sequence fitting were selected originally on the basis that their parallaxes were of the highest precision available. Thus, as with astronomical site testing, there is likely to be a bias towards over-optimism, that is, stars where the measured parallax, π, and hence $\frac{\sigma_\pi}{\pi}$, is overestimated. Therefore, as more

parallax data of higher accuracy are accumulated, one expects π to decrease as it converges towards π_0, and the inferred absolute magnitude to become brighter. A comparison of the various absolute magnitudes cited in the astronomical literature for the "classical" subdwarfs, such as HD 201891 and HD 1394439/40, shows that this is indeed the case, and with Hipparcos providing up to a factor of ten increased accuracy, it is not surprising that the trend continues.

Figure 2a compares the new Hipparcos data against the absolute parallax measurements listed for 26 stars in the YPC. The formal uncertainties in the YPC measurements range from 1.5 to 15 milliarcseconds (mas), and the mean difference between the two datasets is -0.60 ± 5.09 mas. The trend towards negative residuals at smaller π_{abs}(YPC) reflects our selection of only the higher-precision parallaxes: the Hipparcos parallaxes for stars with π(YPC) > π(Hip) and π(YPC) < 10 mas are less precise than 20% cutoff we have imposed on our sample. Note, however, the tendency towards positive residuals amongst the stars with larger YPC parallaxes. In nine out of the eleven cases where the YPC parallax exceeds 15 mas, the Hipparcos parallaxes are smaller.

This offset towards smaller parallaxes and larger inferred distances can be explained to a large extent by the higher accuracy of the Hipparcos data, and the consequent reduction in the necessary systematic (Lutz-Kelker) parallax corrections that are required for statistical analysis. However, given the small number of calibrators available to previous studies, significant offsets in the mean M_V calibration can persist even after allowing for LK effects. As an example, figure 2b compares the ground-based and Hipparcos LK-corrected absolute magnitudes for nine subdwarf included as calibrators by S96 in their study of M5. Eight of these stars have high-precision Hipparcos parallax measurements, and we have also plotted data for HD 219617, although the substantial uncertainty in even the Hipparcos parallax leads to its exclusion from any further statistical analysis. The mean offset in absolute magnitude between the two datasets for the eight high-precision subdwarfs is 0.094±0.094, in the sense that the Hipparcos stars are brighter. Including HD 219617, the mean magnitude difference, ΔM_V, becomes 0.159±0.105 magnitudes. We also compare in figure 2b the S96 and YPC LK-corrected absolute magnitudes for HD 25329, 134439 and 134440. While there is little difference in the case of HD 25329, the final YPC data lead to absolute magnitudes for the last two stars which are 0.1 magnitude brighter than those adopted by S96.

The mean residuals between the S96 and Hipparcos-based absolute magnitudes are formally consistent at the 1σ level. However, note that S96 based their selection of the Hanson $n = 2$ LK corrections on the proper-motion distribution of their subdwarf calibrators. As described in the previous section, the bias towards higher-precision

measurements amongst those stars could lead to adopting too small a value of n. If we recalculate M_V^{LK} for the S96 stars using $n = 3$, the mean difference is only 0.04 magnitudes; for $n = 3.4$, the difference is +0.02 magnitudes. In any case, the presence of this systematic difference between the (significantly more accurate) Hipparcos measurements and the S96 parallax dataset has obvious repercussions for determining the distances of globular clusters.

2.3. The metal-poor main-sequence

Most of the subdwarfs in the current sample have accurate photometric observation in the UBV passbands. This is unfortunate, since the relatively steep slope of the (M_V, (B-V)) main-sequence and the sensitivity to line-of-sight absorption are significant factors in estimating distances to many clusters, as is discussed further in the following section. However, we can at least use our data to provide an empirical definition of the position of the upper main-sequence as a function of abundance.

Figure 3 plots the (M_V, $(B\text{-}V)_0$) colour-magnitude diagram defined by the stars in our sample with high-precision ($\frac{\sigma_\pi}{\pi} < 12\%$) trigonometric parallaxes. We have used different symbols to identify stars within different abundance ranges, and have also plotted data for subdwarfs with -1.0 $\leq$ [Fe/H] ≤ -1.25 and for stars within 30 parsecs of the Sun which are included in our subset of the Hipparcos catalogue. The most significant feature of this diagram is the small separation in M_V between the [Fe/H]~ -1.75 and [Fe/H] < -2 subdwarfs. As discussed further in sections 3.3 and 4.2, where we compare our data against model isochrones, this suggests that current models overestimate the change in luminosity with decreasing abundance for extreme metal-poor subdwarfs. [Fe/H]=-2.0 subdwarfs are not as subluminous as expected. Again, this has clear implications for the cluster distance scale.

3. Globular cluster distance determinations

The high-precision parallax subdwarfs listed in Table 1 span a range of almost 1 dex in [Fe/H] and absolute magnitudes from M_V=+4 to +7, defining the upper main-sequence for intermediate and extreme low-abundance systems. We can supplement these observations with data for three other subdwarfs with accurate ground-based parallax measurements: the intermediate subdwarf binary HD 134439/134440 ($\frac{\sigma_\pi}{\pi} = 0.05$); and the extreme subdwarf HD 25329 ($\frac{\sigma_\pi}{\pi} = 0.03$). We have taken the photometry and abundance estimates for the latter three stars from S96, while the parallaxes are from the YPC.

3.1. Main-sequence fitting

We have matched the local calibrators against fiducial colour-magnitude sequences determined for seven globular clusters - the intermediate abundance systems M5 (S96), M13 (Richer & Fahlman, 1986; Sandage, 1970 (subgiant and RGB)) and NGC 6752 (Penny & Dickens, 1985); and the metal-poor systems M30 (Richer, Fahlman & Vandenberg, 1988), M92 (Stetson & Harris, 1988), M15 (Durrell & Harris, 1993; Fahlman, Richer & Vandenberg, 1985) and M68 (McClure et al, 1987). All have (B, V) CCD photometric observations which extend well below the main-sequence turnoff. (Most, unfortunately, have *only* published BV observations.) While all of these clusters lie at moderate to high galactic latitude, at least three clusters have significant foreground reddening. Determining the magnitude of foreground reddening is not straightforward, and the value adopted can have a significant impact on one's conclusions, as will become apparent. Two widely used estimators, which have the advantage of being available for most clusters, are Burstein & Heiles (1982) HI maps and Zinn's (1980) analysis of reddening-free colour indices derived from integrated photometry. The uncertainties associated with the individual measurements on either scale are ± 0.02 to 0.03 mag, so the two sets of results are in statistical agreement. However, a difference of 0.05 mag in E_{B-V}, as is the case for M68, has a substantial effect on the derived intrinsic luminosity of the horizontal branch and the colour at the turnoff, and hence the inferred age.

Of the seven clusters in our sample, there is general agreement that M5, M13 and M92 have little foreground absorption, but there is less than unanimity on the appropriate reddening for the other four clusters. Table 2 lists other reddening estimates for those systems. We have not included any estimate based on inter-cluster comparisons, since those are generally predicated on the assumption that clusters of the same abundance have identical colours at the turnoff (i.e. identical ages). This technique obviously hampers the prospect of detecting age differences between clusters. Thus, we have concentrated on results based on the photometric properties of horizontal branch stars or nearby field stars. As with the Burstein & Heiles and Zinn results, the derived reddenings span a range of $\sim$0.04 magnitudes for an individual cluster, even if based on the same method. Thus, Brocato et al (1994) estimate a reddening of $E_{B-V} = 0.03$ mag towards M68 (and 0.07 towards M15) based partly on the colour of the blue edge of the RR Lyrae instability strip; Walker (1994), who has undertaken the most thorough examination of this issue, estimates $E_{B-V} = 0.08$ mag from the same parameter (derived directly from his photometry). Walker's final estimate of $E_{B-V} = 0.07 \pm 0.01$ mag for M68 is clearly better supported observationally than is the lower value favoured by Brocato et al.

Clearly, deep I-band and infrared (JHK) photometry would serve to minimise these

problems. However, lacking such data, we have matched the cluster sequences to the local calibrators for a range of assumed values for the foreground absorption, listed in Table 3. In particular, for the metal-poor clusters, the three values adopted for E_{B-V} represent the maximum and minimum likely reddening, and a median value which results in a colour-magnitude diagram that is in close agreement with the de-reddened M92 fiducial sequence. The three low-reddening clusters, M5, M13 and M92, serve as our prime references for comparisons with theoretical isochrones and for age determinations.

Table 3 also gives the Zinn & West (1984 - ZW84) abundance estimates for each system. Recently, Carretta & Gratton (1997) have published abundances for 24 clusters, including all five in our sample, based on high-dispersion spectroscopy. Their results are within 0.1 dex of the ZW84 scale for the metal-poor clusters, but indicate metallicities that are ~ 0.2 dex higher than the ZW84 values for M5, M13 and NGC 6752. Were we to adopt these higher abundances for the latter clusters, then we should also calibrate their distances using higher-abundance subdwarfs, and would expect to derive distance moduli that are larger by 0.05 to 0.1 magnitudes. However, the issue is complicated further by the fact that Balachandran and Carney (1996) have used echelle spectra to derive an abundance of -1.22 for HD 103095 - that is, 0.2 dex higher than the CLLA analysis. Given that most of the calibrating subdwarfs in Table 1 lack high-dispersion spectroscopy, we have adopted the ZW84 and CLLA abundance scales respectively for the clusters and subdwarfs in the current analysis.

We have adjusted each of the observed (V, B-V) fiducial sequences to intrinsic colours and magnitudes using the reddenings listed in Table 3, adopting a value of 3.1 for the ratio of total to selective extinction. The best-fit distance modulus is determined by (linearly) minimising the residuals in (V_0-M_V) with respect to the relevant subset of primary calibrators. In the case of M5, the latter stars span the abundance range -1.25 < [Fe/H] < -1.6; for M13, we adopt abundance limits of -1.4 < [Fe/H] < -1.85; and we include all stars with [Fe/H] > -1.7 for the three extreme metal-poor clusters. In the fitting process, each star is weighted by the uncertainty in its absolute magnitude - that is, the residuals are normalised based on the individual values of σ_M.

In this initial analysis, we have not applied the usual colour-correction technique to adjust all of the stars to the same effective abundance, since the small abundance range in each sub-sample means that the maximum correction is less than 0.015 magnitudes in (B-V). We have, however, estimated the effect of errors in the subdwarf colours by applying systematic offsets of ± 0.02 magnitudes in (B-V) to *all* of the calibrators in each group. As one might expect given the steep slope of the (M_V, (B-V)) main-sequence, these offsets lead to a typical change in distance modulus of ~ 0.14 magnitudes, in the sense that making

the subdwarfs bluer reduces the inferred distance. Changing the reddening by ±0.02 mag generally leads to somewhat smaller changes in distance modulus (±0.1 mag), since the change in V_0 counteracts to some extent the shift in colour, δE_{B-V}, of the de-reddened cluster sequence. A lower value for the reddening leads to a smaller distance modulus, and an inferred fainter intrinsic luminosity at the cluster turnoff. The change in distance modulus also depends on the distribution of calibrating subdwarfs, however, and, with more higher-luminosity calibrators (at colours where the main-sequence is steepening), distance determinations to the extreme metal-poor clusters are more sensitive to changes in the foreground reddening.

Figures 4 and 5 show the results of the main-sequence fitting. In each case, we plot the calibrating subdwarf data together with the individual cluster colour-magnitude diagrams offset by the best-fit distance modulus, $(m\text{-}M)_{12}$ (Table 3). The upper panel in figure 4 plots the calibrated NGC 6752 colour-magnitude diagram for the two estimates of the reddening given in Table 3, while the separate panels in figure 5 show results of adopting either the mean or maximum reddening values for the metal-poor systems. Clearly, the distance moduli that we derive for the latter clusters are dependent sensitively on the adopted extinction, a matter we discuss further in the following section while comparing our new results to older analyses. However, note that adopting the minimum possible value of E_{B-V}=0 for M92 reduces the derived distance modulus by only 0.07 magnitudes, to 14.86 magnitudes.

3.2. A comparison with previous distance determinations

Table 3 presents distance determinations derived from previous studies of the clusters in our sample. In the case of the intermediate abundance systems, our new results differ by no more than ~ 0.15 magnitudes from currently-accepted values. This is clearly comparable to the offset between the S96 and Hipparcos-based absolute magnitudes, as shown in figure 2. However, one should note that the S96 analysis of M5 is based on the high-dispersion abundance estimate of [Fe/H]=-1.19. Dropping the abundance to [Fe/H]$\sim$-1.4, as in our analysis, reduces their derived distance modulus by ~ 0.1 magnitude and increases the disparity with respect to our result. As regards M13 and NGC 6752, two clusters with similar abundances, we note that aligning the fiducial sequences in colour at the turnoff (i.e. $E_{B-V} = 0.02$ mag for NGC 6752) leads to an offset of ~ 0.15 magnitudes on the subgiant branch (NGC 6752 fainter) and an ~ 0.05 magnitude difference in the colour of the giant branch. A direct comparative photometric study of these two clusters would clearly help settle whether the morphological differences in the shape of the turnoff region reflect

intrinsic differences or subtle problems with instrumental calibration.

Reddening is clearly an important factor in the analysis of several of the metal-poor clusters (figure 5). Nonetheless, all of our derived distances are larger than previous determinations. Given these differences, we have tested the robustness of our conclusions by re-analysing the [Fe/H]<-2.0 cluster data (particularly M92), modifying both the set of stars in the calibrating sample and the distance-determining technique. First, we have limited the subdwarf calibrators to only those stars with [Fe/H] < -2, thereby eliminating the influence of the three slightly more metal-rich subdwarfs at (B-V)$\sim$ 0.6. The best-fit distance moduli are reduced, but by only $\sim$0.03 magnitudes. Indeed, matching M92 against either subdwarfs in the abundance range -1.7 < [Fe/H] < -1.95 gives $(m\text{-}M)_0$=14.92, further emphasising our comments of section 2.3 on the apparent "saturation" of subluminosity with decreasing abundance.

Second, eleven stars (four primary and seven secondary calibrators) listed in Table 1 are identified by CLLA as suspected or confirmed single-lined binaries based on their radial velocity measurements, while analysis of the Hipparcos astrometry leads to three other stars being suspected as non-single. [3] As single-lined stars, several may have companions that are substantially less massive, but one of the suspected binary stars is HD 84937 (M_V=3.73), which appears over-luminous for its colour when compared against the cluster sequences. However, excluding all possible binaries from the main-sequence fitting affects the derived distance moduli at only the $\pm$0.05 magnitude level.

Third, cluster main-sequence fitting analyses usually exclude subdwarf calibrators with $M_V < 5.5$ on the basis that the position in the HR diagram of these stars is dependent on their age. The evolutionary variation in (B-V) colour is less than 0.02 magnitudes for $M_V > 4.5$ and ages of less than 10 Gyrs, however. Furthermore, if the subdwarfs are younger than the clusters, then they lie blueward of the correct isochrone and will lead to an underestimate of the distance and an overestimate of the age. Given the many other uncertainties in the main-sequence fitting process, there is little justification for excluding stars such as HD 19445 from the analysis on the basis of possible evolutionary effects. (A more valid reason is the steepness of the main-sequence at these magnitudes, and consequent sensitivity to inaccurate photometry.) In any event, excluding all metal-poor stars with $M_V < 5.5$ (whose position in the H-R diagram is dependent significantly on age) from the calibrating sample still leads to a best-fit distance modulus of 14.9 magnitudes for M92.

[3]Twelve potential single-lined binaries amongst 35 halo subdwarfs is a surprisingly high fraction, given that CLLA cite an overall spectroscopic-binary frequency of only 15 % for metal-poor stars.

Fourth, we can take the opposite approach, and use only HD 19445 as a distance estimator. The abundance is a close match to the metal-poor clusters; it has a well-defined absolute magnitude of $M_V = 5.12 \pm 0.09$; there is no evidence that HD 19445 is an unresolved binary star; and, as we noted above, if HD 19445 will only lead to an overestimate of the cluster distance if it is older (redder) than the cluster stars. Hence, this star can be taken as representative of an unevolved, extreme F-type subdwarf. The M92 fiducial sequence crosses (B-V)=0.477 ($(B-V)_0$=0.457) at V=20.0. Comparison with HD 19445 alone then gives a distance modulus estimate of ~ 14.80 - substantially higher than the 14.65 derived by Bolte & Hogan (1995). Thus, the metal-poor stars in the Hipparcos sample define an empirical main-sequence which is well-matched to the M92-like cluster main-sequence at all colours.

As an alternative to trimming the number of calibrators, we have repeated the main-sequence fitting using the complete sample of subdwarfs listed in Table 1. We have used the same abundance limits as in the analysis based on the primary calibrators, again using the uncorrected (B-V) colours for the subdwarfs. The derived distance moduli are listed in Table 2 as $(m-M)_{20}$. All indicate higher distances than the analysis limited to the high-precision stars.

A systematic difference between our photometric data and the magnitudes and colours used in previous analyses would produce a systematic difference in the estimated distance. Our (B-V) colours and V magnitudes are taken from CLLA. While there is excellent agreement between the magnitudes in the latter catalogue and the data listed both in the Hipparcos catalogue and by S96, the (B-V) colours for a few stars differ by 0.02 to 0.03 magnitudes. However, in almost every case, the difference is in the sense that the CLLA colours are *bluer*. Thus, if we were to adopt the alternative colour estimates, the distance moduli would be driven to larger values, by from 0.1 to 0.15 magnitudes.

As a final test, we have used theoretically-based colour correction to derive mono-metallicity subdwarf sequences, and matched these against the cluster data. First, we have limited our sample to primary Hipparcos calibrators with $[Fe/H] < -1.35$ (i.e. all save HD 194598). Following S96 and BH95, we have used the BV92 theoretical isochrones to compute the differential colour corrections required to place all of those stars on an [Fe/H]=-2.1 main sequence. The required corrections, δ_{B-V}, are listed in Table 1. We then used the same minimisation technique to match the (V_0, $(B-V)_0$) fiducial sequences of the metal-poor clusters to the mono-metallicity subdwarf distribution. The resulting distance moduli, $(m-M)_{-2.1}$, are listed in Table 2, and figure 6 compares the calibrated sequences and the calibrators. While this fitting technique does produce lower distance estimates, the reduction in $(m-M)_0$ is only $\sim$0.1 magnitude.

We have also undertaken the same analysis using a subset of the S96 subdwarfs as calibrators. Rather than basing the calibration on stars with the highest-precision parallax measurements, we have selected a sample of metal-poor stars with parallaxes of at least moderate accuracy. Limiting the calibrating sample to the more metal-poor stars limits the required colour corrections. Figure 1 shows that the difference between the $n = 2$ and $n = 3$ Hanson formulations is only 0.06 magnitudes at $\frac{\sigma_\pi}{\pi}$=15%. Thus, systematic errors in the Lutz-Kelker corrections are not a significant factor for stars with parallaxes of this precision. S96 include eleven subdwarfs in their compilation (including HD 103095) with parallaxes satisfying that criterion and with [Fe/H]<-1.3. We have used these stars to calibrate the distance to M92, taking the relevant data directly from Table 9 of S96. We have adopted both their (B-V) colours, adjusting each to [Fe/H]=-2.1 using the BV92 isochrones, and the LK-corrected absolute magnitudes listed in that paper (i.e. for a Hanson n=2 model). We have not adjusted the parallax measurements of HD 25329, 134439 and 134440 to the YPC values, but applying our fitting technique, we derive a best-fit true distance modulus of 14.82 for M92 (figure 7). D'Antona et al (1997) have derived similar results based on comparable pre-Hipparcos, deriving a a distance modulus of 14.80 magnitudes for M92. As they note, HD 103095 falls ~ 0.2 magnitudes below the main-sequence if one minimises the residuals (V_0 - M_V) with respect to *all* of the subdwarfs in the sample.

Thus, all of the analyses based on the new Hipparcos parallax data, and even analyses based on the average of the older ground-based data, indicate that the current estimates of the distances of intermediate-abundance ([Fe/H]~ -1.5) clusters may require adjustments of up to 6 %, while those to the metal-poor clusters M92, M15, M30 and M68 fall short of the mark by 15 to 20 %.

3.3. Empirical vs. semi-empirical distance estimates

Why are our current distance modulus estimates so much larger than most previous estimates? There are three main reasons: the higher accuracy and precision of the new observations; the larger range in M_V spanned by the new data; and, most important in the case of the extreme metal-poor clusters, the increased number of [Fe/H]<-1.7 calibrators, eliminating the necessity for theoretically-based colour corrections.

In most previous studies, the distance modulus derived from main-sequence fitting rests on only 7 to 10 calibrating parallax stars. For example, Bolte & Hogan (1995) relied on ten nearby subdwarfs in calibrating the distance to M92. Seven of these stars have [Fe/H] > -1.5, and only two of the ten are more luminous than M_V=6. The S96 compilation of ground-based parallax data represented a significant improvement over previous studies,

but even this sample of 23 stars includes only seven with parallax uncertainties of better than 7 %. In contrast, eight stars have $\frac{\sigma_\pi}{\pi} > 20\%$, including three of only seven stars with [Fe/H]<-2. As figure 1 shows, these last stars lie in a régime where the predicted LK corrections are dependent strongly on the functional form assumed for the parallax distribution of the parent sample, and the inferred absolute magnitudes are correspondingly uncertain. Finally, four of the high-precision stars have [Fe/H]>-1.6. Hence, in matching a metal-poor cluster, one is dependent on the accuracy of the colour corrections applied to the latter stars which, as the most accurate, dominate any least-squares fitting process.

To demonstrate the problems faced by previous studies, figure 8 plots the (M_V, (B-V)) colour-magnitude diagram described by the ten calibrators used by Bolte & Hogan (1995) in their study of M92. We have indicated the abundance of each star and plotted the [Fe/H]=-1.48 and -2.26 12, 14 and 16 Gyr. isochrones from the BV92 models. As discussed further below, the latter have an enhanced oxygen abundance (of [O/Fe]=+0.6 at [Fe/H]=-1.48 and +0.75 at -2.26), but do not allow for any enhancement of the α-elements (Si, Ca, Ti etc). However, apart from the most luminous star, HD 201891, there appears to be good agreement between the [Fe/H]$\sim$-1.4 subdwarfs (which dominate the sample) and the [Fe/H]=-1.48 isochrone. Given this agreement, it is not surprising that, after computing colour corrections from the BV92 models, the mono-metallicity [Fe/H]=-2.26 subdwarf sequence (open circles in figure 8) is a good match to the [Fe/H]=-2.26 BV92 isochrone. Bolte & Hogan adopted the semi-empirical approach of adjusting the BV92 isochrones by +0.015 in (B-V) to fit HD 103095, the star with the most accurate parallax measurement, and then determined the distance modulus to M92 ($(m\text{-}M)_0$=14.65) by fitting the de-reddened cluster sequence to the isochrone data.

Thus, Bolte & Hogan's result is crucially dependent both on the accuracy to which the BV92 isochrones match subdwarfs of the same abundance, and on the accuracy to which HD 103095 ([Fe/H]=-1.44) can be transformed to match the (B-V) colours of an [Fe/H]=-2.26 subdwarf. The Hipparcos data allow us to test these hypotheses by comparing the BV92 (M_V, (B-V)) isochrones directly against the distribution of the local subdwarfs. Figure 9 shows this comparison for isochrones of four specific abundances. In each case, we have included the 12, 14 and 16 Gyr isochrones presented by BV92 without any adjustment to the (B-V) colours, and plot both primary and secondary subdwarf calibrators (from Table 1) of similar abundance. We have also plotted the colour-magnitude diagram for the appropriate low-reddening cluster at $(m\text{-}M)_{12}$. It is clear that the BV92 isochrones are significantly bluer than the subdwarf data at all abundances. Specifically, the [Fe/H]=-2.26 isochrones are $\sim$ 0.06 magnitudes bluer than the calibrated M92 sequence at M_V=6.5, the absolute magnitude of HD 103095. Thus, adjusting these isochrones by only +0.015 leads to an offset of $\Delta M_V \sim +0.2$ magnitudes, and a correspondingly smaller distance modulus

when one matches the isochrones against the M92 data. Since the isochrones are too blue for the unevolved stars, matching the colour at the turnoff inevitably leads to age estimates of more than 14 Gyrs.

Increasing the [α/Fe] ratio in these models mitigates the offset in colour to some extent, since an enhanced α-element abundance moves a model of given age and abundance to redder colours and fainter magnitudes. A full set of models remains to be calculated, but preliminary calculations by Vandenberg (reported by S96) show a systematic offset of up to ~ 0.03 magnitudes in (B-V) for intermediate-abundance lower main-sequence stars (S96, figure 16). The [Fe/H]=-1.31 α-enhanced isochrones lie close to the oxygen-enhanced [Fe/H]-1.03 BV92 tracks. S96 used Vandenberg's calculations to determine a distance modulus of $(m\text{-}M)_0 = 14.41$ for M5 (and an age of 12 Gyrs). This is significantly closer to the result that we derive by direct comparison against the local subdwarf stars.

The comparison plotted in figure 9 clearly invalidates the direct use of the BV92 isochrones to determine cluster distance moduli (as in Durrell and Harris, 1993). However, the subdwarf data also suggest that these models may not be well suited for the calculation of the differential colour corrections required to adjust stars to an extremely metal-poor mono-metallicity sequence. As already noted in section 2.3, there is relatively little change in δM_V, the distance that a star falls below the solar-abundance main sequence, for [Fe/H] < -1.5 dex. As we have already noted, the best-fit M92 distance modulus is essentially identical whether one uses the most metal-poor stars or -1.7 < [Fe/H] < -1.95 subdwarfs as calibrators. One might attribute this to problems in the abundances derived for the metal-poor subdwarfs that have been added to the "classical" calibrators. However, HD 103095, HD 64090 and HD 25329 give individual distance estimates to the intermediate-abundance cluster M13 which agree to within 0.05 magnitudes despite the difference in abundance amongst the subdwarfs. Indeed, even using only HD 19445 ([Fe/H]=-2.1) as a calibrator changes the inferred distance modulus to M13 by -0.15 magnitudes. This is less than the $\sim 0.25 - 0.3$ magnitudes one would expect based on the theoretical isochrones and, again, suggests that the BV92 isochrones may overestimate the variation in luminosity and colour at the lowest abundances.

3.4. Summary

It is clear that the currently-accepted distances to the metal-poor clusters are tied closely to the assumption that standard stellar models (particularly the BV92 dataset) provide an accurate representation of the colour-magnitude distribution of metal-poor stars. The Hipparcos data indicate that this is not the case. Empirical distance determinations,

even based on a suitably chosen sample drawn from the S96 calibrators, lead to higher distance moduli for most the globular clusters in our sample. It is also clear that foreground reddening introduces significant uncertainties in the distance determination, particularly for the more metal-poor systems.

Taking these considerations into account, we have adopted the $(m\text{-}M)_{12}$ distance moduli listed in Table 3 as our current best estimate of the distances of the seven clusters in the current sample. Of the three distance estimates given for M15, M68 and M30, we regard the low-reddening value as the least likely, and take the median value as our reference point. The continued scarcity of extremely metal-poor stars with high-precision parallaxes means that the distances to the [Fe/H]$\sim$-2.1 clusters are least well determined. Tying the distances to HD 19445, rather than to the average of the extreme metal-poor calibrators, decreases the distance moduli by 0.12 magnitudes. We regard this as an upper limit to the likely systematic errors in the distances to these clusters.

Summarising, we find M5 and M13 to lie at respective distances of 7.8 and 7.9 kpc (distance moduli of 14.45 and 14.48), and the distance to NGC 6752 is estimated as 4.3 kpc. Adopting the median reddening estimates for M68, M15 and M30, we place these clusters at distances of 11.4, 11.9 and 9.8 kpc ($(m\text{-}M)_0$ = 15.29, 15.38 and 14.95), while M92 is estimated to be at a distance of 9.7 kpc (distance modulus of 14.93 mag). Our estimated random uncertainties in these values are $\pm$0.1 mag in $(m\text{-}M)_{12}$, or $\pm$5% in distance.

4. Discussion

Based on the analysis presented in this paper, we have arrived at the conclusion that the metal-poor globular clusters lie at larger distances than was accepted previously. The discrepancies are particularly pronounced for the extreme metal-poor systems, where our estimates exceed the standard value by $\sim$ 15%. This conclusion obviously affects the luminosities that one derives for stars in these clusters, specifically on the horizontal branch and at the main-sequence turnoff, and adjusting the latter clearly affects the age that one infers for these systems. Our revised distances also suggest that the globular clusters are younger than the currently-accepted value of $\sim$16 Gyrs. Feast & Catchpole (1997) have arrived recently at similar conclusions, but through a complementary series of observations. They have used their proposed revision of the distance to the LMC to infer the absolute magnitude calibration of RR Lyrae variables, and thence re-determine distances to globular clusters. Our analysis runs in the opposite direction: we use our distance estimates to the globular clusters to infer the RR Lyrae absolute magnitude calibration, and the distance modulus of the LMC. In this section we explore some of the immediate repercussions of this

re-calibration of the cluster distance scale.

4.1. The absolute magnitude of RR Lyraes and the distance to the LMC

Moving the globular clusters to larger distances results in an increased luminosity for the horizontal branch stars, and implies a change in the RR Lyrae (M_V, [Fe/H]) calibration. The horizontal branch in M13 lies predominantly blueward of the instability strip, and few variables have been detected. However, four of the remaining clusters all have populous, well-studied RR Lyrae populations.

Considering first the metal-poor clusters, Carney et al (1992b) have presented BV photometry of seven RR Lyraes in M92, and the resultant mean (intensity-weighted) magnitude is $< V >= 15.103 \pm 0.027$. Allowing for a reddening of $E_{B-V} = 0.02$ mag., and adopting a true distance modulus of 14.93 magnitudes, we derive a visual absolute magnitude of $M_V = 0.11$ magnitudes. Walker (1994) derives a mean apparent magnitude of 15.64 magnitudes from observations of 40 stars in M68. Combined with the mean value for the line-of-sight extinction of $A_V = 0.15$ mag and $(m\text{-}M)_0$=15.29, the inferred absolute magnitude is M_V=0.20 magnitudes. The RR Lyraes in the third metal-poor cluster, M15, have been surveyed most recently by Silbermann & Smith (1995), and their observations give a mean magnitude of $< V >= 15.83 \pm 0.09$ mag for 28 stars with well-defined light curves, implying M_V=0.18, for the mean extinction solution ($E_{B-V} = 0.09$ mag) listed in table 3.

The extensive M5 RR Lyrae population has been studied in detail most recently by Reid (1996), who used CCD observations to map the light curves of over 50 stars. Those data give (intensity-weighted) mean apparent magnitudes of $< V >= 15.059 \pm 0.064$ for 33 RRab variables and $< V >= 15.039 \pm 0.037$ for 11 RRc variables. (These averages exclude five higher-luminosity variables which may be on the return traversal of the horizontal branch.) S96 derive similar mean magnitudes from their less extensive CCD observations of a smaller sample of variables. Combined with a reddening of 0.03 magnitudes and $(m\text{-}M)_0$ = 14.45 mag., the latter estimates give gives $M_V = 0.51$ magnitudes.

Figure 10 compares these two absolute magnitude estimates against several recent proposed (M_V, [Fe/H]) calibrations. Our results imply a luminosity-abundance dependence in the absolute visual magnitudes of RR Lyrae variables which is steeper even than that derived by Sandage (1993), although we would emphasise that there is no compelling evidence that this relation should be extrapolated linearly into the metal-rich ([Fe/H] >-1) domaine. If the correlation were to flatten significantly for [Fe/H]>-1.6, then the

current results may well be consistent with the Layden et al statistical parallax analyses. Two-thirds of the local halo RR Lyraes fall in this intermediate abundance range, and have a correspondingly large influence on the mean absolute magnitude derived for the sample as a whole.

In any case, if we assume that the RR Lyraes in metal-poor LMC clusters are similar to the Galactic variables, we can use our results to estimate a distance to the LMC. Walker (1992) lists intensity-weighted average magnitudes for variable in five LMC clusters with [Fe/H]=-1.8±0.1. His analysis is based on only nine star for NGC 2210, but Reid & Freedman (1994) provide average magnitudes for over 30 cluster members, and combing these datasets gives the mean magnitude of $< V_0 >= 18.98$ cited in the introduction. Interpolating in metallicity between the two datapoints defined by our observations - $M_V \sim 0.1 \pm 0.1$ at [Fe/H] ~ -2.1 and $M_V \sim 0.51 \pm 0.1$ at [Fe/H] ~ -1.4 leads to an absolute magnitude estimate of $M_V \sim 0.3 \pm 0.1$ for the LMC RR Lyraes. This implies a distance modulus of 18.68 mag. Of the two extremely metal-poor clusters surveyed by Walker, NGC 1786 ([Fe/H]=-2.3) has a relatively small RR Lyrae population, and the mean magnitude, $< V_0 = 19.05$ mag, is based on data for only nine stars. The instability strip is better defined in NGC 1841 ([Fe/H]=-2.2), where observations of 22 stars give $< V_0 >= 18.75$ mag, or, comparing the variables directly with the Galactic clusters, $(m\text{-}M)_0 = 18.6$ mag. Weighting these results leads to a mean LMC distance modulus of 18.65 mag, ($r \sim 53.7$ kpc), clearly in good agreement with the Cepheid-based distance scale, particularly given the recent revision to the latter proposed by Feast and Catchpole (1997).

4.2. Globular cluster ages and galaxy formation

4.2.1. Isochrone-based age estimates

The larger distances that we have derived for most of the clusters in our sample inevitably lead to higher luminosities for stars at the main-sequence turnoff and, as a result, implied higher masses and younger ages. The effect is particularly significant for the metal-poor clusters, where our revised distance moduli are higher than currently-accepted values by ~ 0.3 magnitudes. A comparison with the isochrones predicted by theoretical modelling offers the only method of quantifying these differences. The individual stellar model calculations, however, generate luminosities and temperatures as a function of age. These must be transformed to the colour-magnitude plane by applying bolometric corrections and appropriate temperature-colour calibrations before the models can be compared with observations. The (T_{eff}, colour) relations remain somewhat problematical for metal-poor stars, and small inaccuracies in the transformed colours can have a profound

impact on the inferred cluster ages, as is clearly demonstrated by the results plotted in figure 9.

Several recent globular cluster studies (notably BH95, S96) have been based on the Bergbusch and Vandenberg (1992) oxygen-enhanced theoretical isochrones. These calculations have been criticised, however, since the [O/Fe] ratio in the models increases with decreasing abundance, from +0.5 dex at [Fe/H]=-1 to +0.75 dex at [Fe/H]=-2.26. The (T_{eff}, colour) transformation is based on Vandenberg's (1992) formalism, and we have already shown that the isochrones do not match the (M_V, (B-V)) distribution of the local subdwarfs. Given this mismatch, we have considered isochrones generated by two other sets of model calculations.

Straniero & Chieffi (1991 - SC91) have calculated a suite of isochrones for abundances between [Fe/H] = -0.5 and [Fe/H] = -2.3, and for ages of 10 to 20 Gyrs. Their models are "classical" in the sense that they allow for enhanced abundances of neither oxygen nor any of the other α elements. However, both SC91 and DCM point out that, for modelling purposes, the increased abundances of this subset of elements may simply mimic a lesser increase in the overall [Fe/H]. We have allowed for this in matching the models to the cluster colour-magnitude data. The transformation of the SC91 (L, T_{eff}) data to the observational plane relies on relations derived by Vandenberg & Bell (1985) and by Bell & Gustafsson (1978), with the latter adjusted to match the former in the region of overlap. Figure 11 compares the resultant (M_V, (B-V)) isochrones for ages of 10, 12, 14 and 16 Gyrs against the Hipparcos subdwarf sample. These models give a closer match to the stars on the unevolved main-sequence, with a typical offset of only ~ 0.02 magnitudes in colour (or 0.1 to 0.15 in M_V). However, it is not possible to fit simultaneously both the colour at the turnoff (ages $\geq$ 16 Gyrs) and the luminosity of the subgiant branch (ages $\leq$ 14 Gyrs).

We have also compared the Hipparcos-based subdwarf data to the sets of models calculated recently by D'Antona, Caloi & Mazzitelli (1997). These models are "classical" in the sense that there are no specific abundance enhancements. However, there are several significant differences in the theoretical framework as compared with the BV92 or SC91 methodology. First, convection is treated using a full scale turbulence analysis, rather than with the standard mixing-length approximation; second, the effects of helium sedimentation are included; and, third, the models use the equation of state developed by Rogers, Swenson & Iglesias (1996). Taken together, these three changes to the input physics in the models lead to both cooler temperatures and lower luminosities for upper main-sequence stars of a given age.

DCM use the Kurucz (1993) (L, T_{eff}) calibrations to transform the model isochrones to (M_V, (B-V)), and figure 12 plots the local subdwarf data together with their results

for abundances of [Fe/H]=-1.3, -1.5 and -2.0 and ages of 10, 12 and 14 Gyrs. Of the three theoretical analyses discussed here, these models provide the closest match to the main-sequence, turnoff and subgiant branch data. The predicted giant branch is generally too red, but DCM point out that, apart from dealing with the inherent physical uncertainties in modelling evolved stars, the predicted colours can be changed by -0.07 magnitudes simply by adopting the Vandenberg (1992) temperature-colour relation rather than the Kurucz calibration. In general, the isochrones predicted by these models are a good match to the shape of the turnoff region in the colour-magnitude diagrams for M5, M13 and M92, and imply ages in the range 11 to 13 Gyrs.

None of the three models discussed here produces isochrones which are an exact match to the shape of the cluster main sequences. Thus, there is a subjective element involved in assessing which model is the closest match to a given dataset. In comparing observational data to theoretical isochrones in the (M_V, (B-V)) plane, one tends to align the two datasets horizontally. This is misleading, since there is usually a factor of ten difference in the scales on the x- and y-axes, and what appears to be a small offset in M_V can be of considerably more significance than a misalignment in (B-V). Moreover, the disparity in colour between the Kurucz and Vandenberg giant-branch calibrations underlines the continuing problems in defining reliable colour-temperature relations. Bolometric corrections are generally better defined. Thus, matching the models to the data in luminosity/M_V, either using the entire luminosity function or specific features, offers the prospect of a more robust age determination.

Neither SC91 nor DCM calculate theoretical luminosity functions, so we have taken the absolute magnitude at the turnoff, M_V(TO), as our point of reference. The cluster colour-magnitude diagrams are nearly vertical at this point, so the apparent magnitude of the turnoff (the bluest point on the main-sequence) is uncertain by at least ± 0.1 magnitudes. Figure 13 compares our estimates for each cluster against the predictions of the three sets of models discussed here. Since neither the SC91 nor DCM models allow for element enhancement, we have offset the data by +0.15 dex in [Fe/H] when comparing the observations to these theoretical models. In the case of the four clusters where the foreground reddening is a source of significant uncertainty, our results are based on the value of E_{B-V} which aligns the subgiant branch with that of the appropriate reference cluster (M13 or M92). Thus, we adopt the median values for the three metal-poor clusters and the higher reddening for NGC 6752. The open triangles indicate the position of the turnoff for the other suggested values of the reddening towards those clusters.

There are two important conclusions to be drawn from the results presented in figure 13. First, *all* of the age estimates are 14 Gyrs or less - well below the 15.8 Gyr average

found by Bolte & Hogan (1995). The ages derived from the three sets of models for a given cluster (and reddening) also span a relatively small range, with typically only 1-2 Gyrs difference between the ages derived from the classical SC91 models and the (younger) BV92 and DCM age estimates. Note, in particular, that if we adopt the HD 19445 calibration for the metal-poor clusters (i.e ($\delta(m-M)_0 = +0.12$ mag), the average age increases by only ~ 1 Gyr: to 13 Gyrs if calibrated against the SC91 models, and to 12 Gyrs in the case of the BV92 and DCM models.

Second, there is a suggestion of some dispersion in the cluster ages amongst the metal-poor clusters. The age estimates for the three clusters with low extinction, M5, M13 and M92, agree within the 1σ uncertainties irrespective of the model one adopts. However, if we adopt the standard values for the line-of-sight reddening towards M68 and M15 (i.e. $E_B - V = 0.07$ and 0.11 magnitudes, corresponding to the uppermost open triangles plotted in figure 13), then both clusters are significantly (~ 2 Gyrs) younger than M92. DCM arrive at similar conclusions based on their isochrone-fitting of the M68 and M92 colour-magnitude diagrams.

The suggestion of an age-spread amongst globular clusters is by no means unprecedented: Bolte (1989) originally proposed that NGC 362 is 2-3 Gyrs younger than NGC 288, while Buonnano et al (1994) have identified four clusters in the outer halo (Terzan 7, Arp 2, Pal 12 and Ruprecht 106) which appear to be 3-4 Gyrs. younger than 47 Tucanae. All of these clusters have abundances [Fe/H] $>\sim -1.6$, however, and, previous studies of the extreme metal-poor systems are more equivocal. Chaboyer et al (1996) place M68 amongst the youngest Galactic globulars based on the luminosity redward of the turnoff, on the subgiant branch. These results are obviously dependent on the reddening that one adopts, and Vandenberg, Bolte & Stetson (1990) have shown that the colour-difference between the turnoff and the base of the giant branch, a reddening-independent parameter, is identical within the observational uncertainties for M92 and M68. On the other hand, the blue horizontal branch is more extended in both M15 and M68 than in M92, suggesting a possible age difference, and Chaboyer, Demarque & Sarajedini (1996) estimate an difference of 5 Gyrs between the ages of M92 and M68, with M15 having an intermediate age.

In summary, depending on the reddening towards the individual clusters, our data *may* indicate an age spread amongst the metal-poor halo clusters. Irrespective of reddening uncertainties, however, it is clear that the average age of even extreme metal-poor halo globular clusters is significantly less than 14 Gyrs, and may well be as low as 12 Gyrs.

4.2.2. Cluster ages and the early history of the Galaxy

A younger Galactic halo has a number of significant implications for models of Galactic evolution. First, and foremost, one is not faced with the problem of explaining how the Galaxy managed to form a substantial number of halo globular clusters, and perhaps most of the field stars in the halo, during a period of collapse very early in its history, and then allowed the star formation rate to dwindle to insignificant levels for up to 4 Gyrs before embarking on the task of disk formation. The age of the Galactic disk is not yet well defined. However, Oswalt et al (1996) have set a lower limit of 9.5 Gyrs, based on the shape of the white dwarf luminosity function at low luminosities. A small number of open clusters, however, are suspected of dating from the earliest epochs of disk formation, and Phelps (1997) has recently estimated an age of 12^{+1}_{-2} Gyrs for Berkeley 17. This would make this -0.3 $\leq$ [Fe/H] $\leq$ 0.0 cluster a close contemporary of both M5 and M92, systems with abundances lower by almost a factor of 100. This suggests strongly that star formation started at approximately the same time in *both* the halo and disk stellar populations.

Our results also show weak evidence for a spread in ages amongst the metal-poor halo clusters, with the strongest support lying in Walker's (1994) thorough analysis of the reddening towards M68. If confirmed by further observations, this would require the presence of metal-poor gas well after the first outburst of star formation throughout the Galaxy, and after several generations of supernovae and AGB stars have enriched the metal content of the interstellar medium. The most likely mechanism for avoiding pollution by stellar ejecta is to form any younger clusters from infalling primordial gas clouds. This is essentially a minor variation on the theme presented originally by Searle & Zinn (1978). Recent observational studies of distant halo stars, notably by Majewski, Munn & Hawley (1994), have provided evidence for kinematic sub-structure within the halo, suggesting continued accretion of distinct systems. These results have been discussed primarily in the context of mergers of relatively-massive, dwarf spheroidal systems, and the consequent impact on the dynamical evolution of the disk. However, a significant fraction of the halo (which has a total mass only a few percent that of the disk) may well have been constructed over the initial 2-4 Gyr period of the Galaxy's lifetime by the accumulation of gas clouds with individual masses of no more than $\sim 10^6 M_\odot$. Continued accretion also provides a natural explanation for the presence of two distinct kinematic components within the Galactic halo, as proposed by Hartwick (1987) and Sommer-Larsen & Zhen (1990), and supported by Majewski's (1992) detection of retrograde rotation in the outer halo.

As a qualitative outline of the overall formation scheme, we hypothesise that the initial stages of Galactic formation occurred as a rapid collapse, in the manner proposed originally by Eggen, Lynden-Bell and Sandage (1962). During the first few $\times 10^8$ years, star formation

occurred throughout the proto-halo, with the lower angular-momentum processed material falling deeper into the Galactic potential well and enriching the proto-disk (and bulge). Most of the initial star clusters were disrupted to form the field stars in the present Galactic halo.

The infalling gas collapses into a rotating disk, and star formation commences within the disk no more than 0.5 Gyr after the first halo stars formed. The likeliest candidates for first disk stars are the metal-weak "thick disk" stars identified by Morrison, Flynn & Freeman (1990), and it is likely that most of the globular clusters in Zinn's disk system (Zinn, 1985) also formed during this phase of Galactic evolution. The gas within the disk collapses further to form the thin disk - the precursor to the component currently termed the old disk - with mild star formation persists within "thick disk" material, whose larger scaleheight is maintained by continued infall of gaseous material. This accretion of primordial gas-clouds may also lead to the addition of younger, metal-poor globulars, such as M15 and M68, to the outer Galactic halo.

This is an hypothesis which clearly requires more quantitative development. However, the characterisation of galaxy formation as a relatively unspectacular process, involving no more than a moderate star formation rate extending over several Gyrs, and with continued accretion to relatively modest redshifts ($z \sim 2$), is in accord with observations of faint galaxies in the Hubble deep field. In particular, the morphological classification undertaken by van den Bergh et al (1996) shows a higher fraction of merging/interacting systems and fewer grand design spirals than amongst nearby galaxies.

4.3. The extragalactic distance scale and the Hubble constant

Given that we have proposed both a larger distance scale and a younger age for the benchmark globular cluster system, it is incumbent upon us to consider how these results impact on the investigations of the distance scale. Since all current investigations of the Hubble expansion are tied, in some respect, to the distance to the LMC, the net result of our proposed change in the distance modulus is a decrease in the inferred Hubble constant. The longer distance scale, favoured by Tammann & Sandage (1996) is based on a number of indicators, some of which are dependent on the assumed LMC distance, either directly through Cepheid-based distances, as is the case for Type I supernovae distance determinations (Sandage et al, 1996), or indirectly, through calibrations of the distance to M31 and M101. However, Sandage (1997, preprint) has argued that the overall calibration is little-dependent on the distance assumed to the LMC, and the inferred value of H_0 is unaltered at 55 ± 5 km s^{-1} Mpc^{-1}. The implied cosmological time-scale remains consistent

with the revised globular cluster ages presented here.

The expansion time-scale inferred from the short distance-scale ($H_0 > 70$ km s^{-1} Mpc^{-1}), however, is in direct conflict with the > 15 Gyr ages that had been assigned previously to the globular cluster system. The distance to the LMC is the corner-stone of the HST Key Project, since the observed Cepheid period-luminosity relations in external galaxies are all scaled to match the LMC relation. Thus, increasing the distance modulus of the LMC from 18.5 (the value adopted in the analyses to date) to 18.65 increases the distance scale by $\sim 7\%$. Moreover, since the results derived by other methods, such as surface-brightness fluctuations (Tonry et al, 1997) and the Tully Fisher method (Bureau, Mould & Staveley-Smith, 1996), are also usually tied to the Cepheid scale, the distance scale adopted in those surveys must be increased by a similar factor. As an example of the resultant effect on the derived H_0, the "mid-term" value of the Hubble constant presented by Freedman et al (1997), $H_0 = 73 \pm 10$ km s^{-1} Mpc^{-1}, is reduced to $H_0 = 68 \pm 9$ km s^{-1} Mpc^{-1}. This corresponds to an expansion age of 12-13 Gyrs for Ω_0=0.2 and to 10 Gyrs for Ω_0=1 (Freedman, priv. comm.). The former value is not inconsistent with the cluster age estimates discussed in the previous sections.

5. Conclusions

We have used high-accuracy parallax measurements made by the Hipparcos astrometric satellite of nearby halo subdwarfs to refine the definition of the main-sequence for metal-poor stars. Combining these data with previous observations of an additional three stars, we have utilised main-sequence fitting techniques to re-determine the distances of three moderately metal-poor and four extremely metal-poor globular clusters. We find that the distances to the former clusters are underestimated by $\sim 2-5\%$, and that the distances to the extreme metal-poor clusters should be increased by $\sim 15\%$. The main source of the former scale-change rests with the revised zeropoint provided by the Hipparcos parallax data; the larger change associated with the metal-poor clusters reflects the fact that many previous distance determinations were semi-empirical in nature, tied to matching theoretical isochrones whose absolute zeropoint was set by one star, HD 103095. Our new data show that the Bergbusch & Vandenberg (1992) isochrones, used by Bolte & Hogan (1995) in their analysis of M92, are too blue in (B-V) when matched against the subdwarf data. As a result, previously-derived distances were too low and, as a consequence, age estimates too old.

Our revision of the distance scale to globular clusters has two main consequences: first, the luminosity associated with horizontal branch stars is increased, particularly at the

lowest abundances, leading to a re-calibration of the RR Lyrae absolute magnitudes, and an inferred distance modulus of 18.65 to the LMC. This brings the Cepheid and RR Lyrae scales into agreement. Second, the increased luminosity of the main-sequence turnoff implies that the clusters are significantly younger. Matching against evolutionary models calculated by Straniero & Chieffi (1991), Bergbusch & Vandenberg (1992) and D'Antona et al (1997), we derive average cluster ages of $\sim$ 11 to 13 Gyrs. If the standard reddening estimates for M68, M15 and M30 are correct, then these three clusters are $\sim$ 2 Gyrs younger than M92. However, decreasing the reddening by only 0.02 magnitudes brings the colour-magnitude diagrams for all four clusters into close alignment.

Irrespective of the reddening uncertainties, our results imply a significantly younger age for the clusters in the Galactic halo. The more conservative Straniero & Chieffi models indicate an age of $\sim$ 13 Gyrs, while the other two models favour an age of only 12 Gyrs. Coupled with recent results which push back the onset of star formation in the disk, this suggests that the initial epochs of star formation in the disk and halo were separated by only a few hundred million years. Finally, taken together the increased distance scale and the younger ages of the oldest globular clusters succeed in almost reconciling the stellar and cosmological age estimates for the Universe.

We acknowledge the substantial efforts made by the many people who have made the Hipparcos project a striking success. INR would also like to thank Wendy Freedman, Ian Thompson and David Hogg for commenting on earlier versions of this paper; Brian Chaboyer and Francesca D'Antona for comments on theoretical models; Mike Bolte for providing the list of subdwarf calibrators used previously to calibrate the distance to M92; Bob Hanson for further clarifying the problems surrounding applying Lutz-Kelker corrections; and George Preston for throwing the reddening spitball.

REFERENCES

Balachandran, S.C., Carney, B.W. 1996, AJ, 111, 946

Bell, R.A., Gustafsson, B. 1978, A&AS, 34, 229

Bergbusch P.A., Vandenberg, D.A. 1992, ApJS, 81, 163

Bingham, E.A., Cacciari, C., Dickens, R.J., Fusi Pecci, F. 1984, MNRAS, 209, 765

Bolte, M. 1989, AJ, 97, 1688

Bolte, M., Hogan, C.J. 1995, Nature, 376, 399

Brocato, E., Castellani, V., Ripepi, V. 1994, AJ, 107, 622

Bureau, M., Mould, J.R., Staveley-Smith, L. 1996, ApJ, 463, 60

Burstein, D., Heiles, C. 1987, AJ, 1165

Buonnano, R., Corsi, C.E., Fusi Pecci, F., Fahlman, G.G., Richer, H. 1994, ApJ, 430, L121

Cacciari, C., Clementini, G., Fernley, J.A., 1991, ApJ, 396, 219

Carretta, E., Gratton. R.G. 1997, A&AS, 121, 95

Carney, B.W. 1979, AJ, 84, 515

Carney, B.W., Storm, J., Jones, R.V. 1992a, ApJ, 386, 663

Carney, B.W., Storm, J. Trammell, S.R., Jones, R.V. 1992b, PASP, 104, 44

Carney, B.W., Latham, D.W., Laird, J.B., Aguilar, L.A. 1994, AJ, 107, 2240 (CLLA)

Chaboyer, B., Demarque, P., Sarajedini, A. 1996, ApJ, 459, 558

Chaboyer, B., Demarque, P., Kernan, P.J., Krauss, L.M., Sarajedini, A. 1996, MNRAS, 283, 683

D'Antona, F., Caloi, V., Mazzitelli, I. 1997, ApJ, 477, 519 (DCM)

Durrell, P.R., Harris, W.E. 1993, AJ, 105, 1420

ESA, 1997, The Hipparcos catalogue, ESA SP-1200

Eggen, O.J., Lynden-Bell, D., Sandage, A.R. 1962, ApJ, 136, 748

Fahlman, G.G., Richer, H.B & Vandenberg, D.A. 1985, ApJS, 58, 225

Feast, M.W. 1997, MNRAS, 284, 761

Feast, M.W., Catchpole, R.W. 1997, MNRAS, in press

Fernley, J.A., 1993, A&A, 284, L16

Freedman, W.L., Madore, B.F., Kennicutt, R.C. 1997, "The Extragalactic Distance Scale", eds. M. Donahue and M. Livio, Cambridge Univ. Press

Giclas, H.L., Burnham, R. Jr., Thomas, N.G. 1971, Lowell Proper Motion Survey (Lowell Observatory, Flagstaff, AZ)

Gould, A 1995, ApJ, 452, 189

Hartwick, F.D.A. 1987, in The Galaxy, (ed. Gilmore, G., Carswell, R.), Reidel, Dordrecht, p. 281

Hanson, R.B. 1979, MNRAS, 186, 875

Kovalevsky, J. et al 1995, A&A, 304, 34

Kurucz, R. L., 1993, ATLAS9 Stellar Atmosphere Programs and 2 kms^{-1} Grid, (Kurucz CD-ROM No. 13)

Layden, A.C., Hanson, R.B., Hawley, S.L., Klemola, A.R., Hanley, C.J. 1996, AJ, 112, 2110

Lutz, T.E., Kelker, D.H. 1973, PASP, 85, 573

McClure, R.D., Vandenberg, D.A., Bell, R.A., Hesser, J.E., Stetson, P.B. 1987, AJ, 93, 1144

Majewski, S.R. 1992, ApJS, 78, 87

Majewski, S.R., Munn, J.A., Hawley, S.L. 1994, ApJ, L37

Mazzitelli, I., D'Antona, F., Caloi, V. 1995, A&A, 302, 382

Morrison, H.L., Flynn, C., Freeman, K.C. 1990, AJ, 100, 1191

Oswalt, T.D., Smith, J.A., Wood, M.A., Hintzen, P. 1996, Nature, 382, 692

Panagia, N., Gilmozzi, R., Macchetto, F., Adorf, H.M., Kirschner, R.P. 1991, ApJ, 380, L23

Penny, A.J., Dickens, R.J. 1985, MNRAS, 220, 845

Perryman, M. A. C. et al 1995, A&A, 304, 69

Phelps, R., 1997, ApJ, in press

Reid, I.N. 1996, MNRAS, 278, 367

Reid, I.N., Freedman, W. 1994, MNRAS, 267, 821

Richer, H.B., Fahlman, G.G. 1986, ApJ, 304, 273

Richer, H.B., Fahlman, G.G., Vandenberg, D.A. 1988, ApJ, 329, 187

Rogers, F.J., Swenson, F.J., Iglesias, C.A. 1996, ApJ, 456, 902

Sandage, A. 1970, ApJ, 162, 841

Sandage, A. 1986, ARA&A, 24, 421

Sandage, A. 1993, AJ, 106, 703

Sandage, A., Saha, A., Tammann, G.A., Labhardt, L., Panagia, N., Macchetto, F.D. 1996, ApJ, 460, L15

Sandquist, E.L., Bolte, M., Stetson, P.B., Hesser, J.E. 1996, ApJ, 470, 910 (S96)

Searle, L., Zinn., R. 1978, ApJ, 225, 537

Silbermann, N.A., Smith, H.A. 1995, AJ, 110, 704

Smith, H. 1987, A&A, 188, 233

Sommer-Larsen, J., Zhen, C. 1990, MNRAS, 242, 10

Stetson, P.B., Harris, W.E. 1988, AJ, 96, 909

Straniero, O, Chieffi, A. 1991, ApJS, 76, 525 (SC91)

Tammann, G.A., Sandage, A. 1996, IAU Symposium 168, p. 163

Tonry, J.L., Blakeslee, J.P., Ajhar, E.A., Dressler, A. 1997, ApJ, 475, 399

Walker, A.R. 1992, ApJ, 390, L81

Walker, A.R. 1994, AJ, 108, 555

van Altena, W.F., Trueng-liang Lee, J., Hoffleit, D., 1995, The General Catalogue of Trigonometric Stellar Parallaxes (Newhaven: Yale Univ. Obs.)

van den Bergh, S., Abraham, R.G., Ellis, R.S., Tanvir, N.R., Santiago, B., Glazebrook, K.G. 1996, AJ, 112, 359

Vandenberg, D., 1992, ApJ, 391, 685

Vandenberg, D., Bell, R.A. 1985, ApJS, 58, 561

Vandenberg, D., Bolte, M., Stetson, P.B. 1990, AJ, 100, 445

Zinn, R. 1980, ApJS, 42, 19

Zinn, R. 1985, ApJ, 293, 424

Zinn, R., West, M., 1984, ApJS, 55, 45

FIGURE CAPTIONS

Fig. 1.— Lutz Kelker corrections. The solid points mark the systematic offset in M_V as a function of $\frac{\sigma_\pi}{\pi}$ calculated originally by Lutz and Kelker and the solid line shows Smith's (1987) analytic representation of these datapoints. The dotted, long-dashed and short-dashed lines outline the corrections predicted by Hanson's formula for $n = 2$, 3 and 4 respectively, where n is the exponent of a power-law parallax distribution. The $n = 4$ (uniform density) case is equivalent to the original Lutz-Kelker analysis.

Fig. 2.— The lower panel shows a comparison between ground-based parallax measurements and Hipparcos astrometry for 26 stars in common between the current sample and the Yale Parallax catalogue. The upper panel compares the absolute magnitudes adopted by S96 for twelve of the stars used in their M5 distance determination against the Hipparcos data (solid dots) and the final YPC data (triangles). The error bars in this diagram represent the combined formal uncertainties of the two M_V estimates, and the dotted line shows the mean offset between the S96 and Hipparcos calibration, excluding HD 219617.

Fig. 3.— The main-sequence for metal-poor stars, defined by Lowell proper motion stars with measured abundances and Hipparcos parallaxes with precision of at least 12 %

Fig. 4.— Main-sequence fitting for the three intermediate-abundance globular clusters discussed in this paper. The calibrating subdwarfs from the appropriate abundance range are plotted at the appropriate Lutz-Kelker corrected absolute magnitudes, and the errorbars indicate 1σ uncertainties. The NGC 6752 fiducial sequence is plotted for the two reddening values listed in Table 3.

Fig. 5.— Main-sequence fitting for the four metal-poor globular clusters. Again, the relevant set of calibrating subdwarfs is shown. The reddening toward M15, M30 and M68 is not unambiguously determined, so we plot the results for two values of the extinction for those clusters. The upper panel shows the best-fit calibration for the highest reddenings listed in Table 3, while the lower panel plots the results if we adopt the intermediate values. The latter lead to an almost exact alignment of the subgiant branch with the (low-reddening) M92 data.

Fig. 6.— The results of matching the M92 fiducial sequence to an [Fe/H]=-2.1 mono-metallicity subdwarf sequence, using the Hipparcos stars as reference and with the differential colour corrections taken from the BV92 models

Fig. 7.— Main-sequence fitting for M92 using a subset of the S96 subdwarfs as the local

calibrators. The open squares mark the observed positions of those stars *at the Lutz-Kelker corrected absolute magnitudes derived by S96*. The solid points mark the same stars after adjusting the (B-V) colours to match an [Fe/H]=-2.1 isophote. The calibrated M92 fiducial sequence is plotted together with the BV92 [Fe/H]=-2.26 14 Gyr isochrone.

Fig. 8.— A comparison in the (M_V, (B-V)) plane between the BV92 oxygen-enhanced isochrones and the location of the ten subdwarf calibrators available to Bolte & Hogan (1995). The solid points mark the actual colours and magnitudes while the open circles show positions after adjusting to [Fe/H]=-2.26. Each subdwarf is labelled with its metallicity, and the three isochrones plotted for each abundance are for ages of 12, 14 and 16 Gyrs. The M92 fiducial sequence is plotted for a distance modulus of 14.65 mag, as derived by BH95

Fig. 9.— A comparison between the BV92 theoretical isochrones and the empirical main-sequence (M_V, (B-V)) defined by the local subdwarfs. Each sub-panel plots 12, 14 and 16 Gyr isochrones for a given abundance, together with the subdwarfs within the specified abundance range and the appropriate globular cluster fiducial sequence. Note that the cluster data are matched to the subdwarfs, not the isochrones.

Fig. 10.— A comparison between the absolute magnitudes we derive for intermediate and extreme metal-poor RR Lyraes based on the distance moduli we derive respectively to M5 and the three clusters M92, M68 and M15. Previously derived (M_V, [Fe/H]) relations are also shown. The solid line marks the results derived by Layden et al from statistical parallax analysis of the local stars, while the dotted lines outline the 1σ uncertainties. We allow for overlap in abundance between their halo and "thick disk" samples. The other linear relation plotted are from Carney et al (1992), Fernley (1994), Sandage (1993) and Feast (1997). The solid points mark our current results.

Fig. 11.— A comparison between the SC91 theoretical isochrones and the empirical main-sequence. As in figure 9, we show a set of model isochrones, in this case for ages of 10, 12, 14 and 16 Gyrs and abundances of [Fe/H]=-1.3, -1.7 and -2.0, together with the relevant subdwarf data and a globular cluster fiducial sequence. The subdwarfs are drawn from the same abundance ranges as in the corresponding panels in figure 9. Since these models do not include any α-element enhancement, we have not plotted the comparison with the [Fe/H]=-2.3 isochrones.

Fig. 12.— A comparison between the DCM theoretical isochrones and the empirical metal-poor main-sequence(s). The format is as in figures 9 and 11, with the theoretical isochrones plotted for ages of 10, 12 and 14 Gyrs and for abundances of [Fe/H] = -1.3, -1.5 and -2.0.

Fig. 13.— Age estimation using the luminosity of the main-sequence turnoff. The observed

values of M_V(TO) are compared to the theoretical predictions of the SC91, BV92 and DCM models. The dotted lines show the predicted variation of M_V(TO) with abundance for a given age (listed on the right edge of each panel). The solid points plot the observed values, with the open triangles showing the effect of adopting the different estimates (given in Table 3) of the reddening towards M15, M68, M30 and NGC 6752. Since neither the SC91 nor DCM models include element enhancements, we have offset the cluster data by +0.15 dex in [Fe/H].

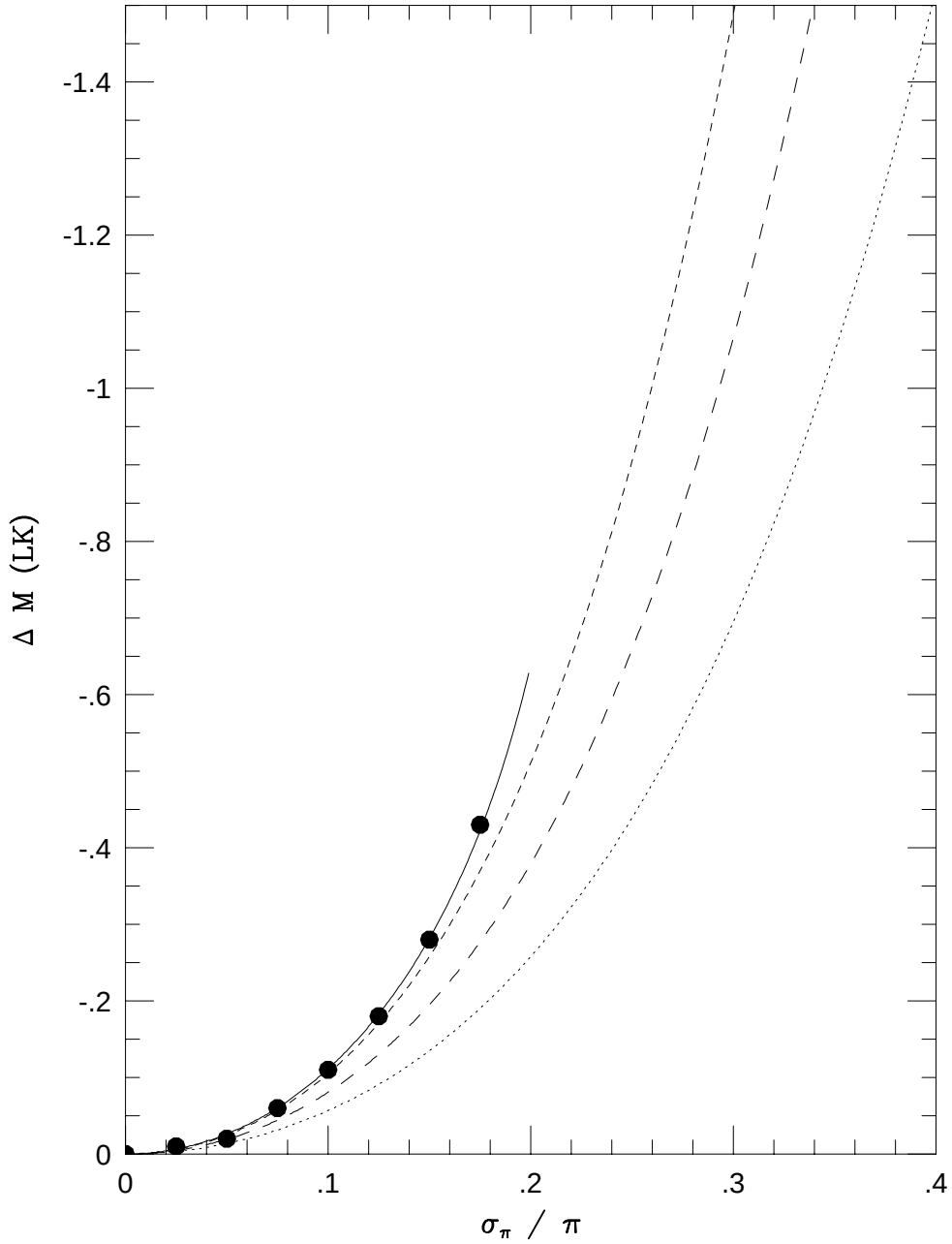

Fig. 1.— Lutz Kelker corrections. The solid points mark the systematic offset in M_V as a function of $\frac{\sigma_\pi}{\pi}$ calculated originally by Lutz and Kelker. The dotted, long-dashed and short-dashed lines outline the corrections predicted by Hanson's formula for n=2, 3 and 4 respectively, where n is the exponent of a power-law parallax distribution.

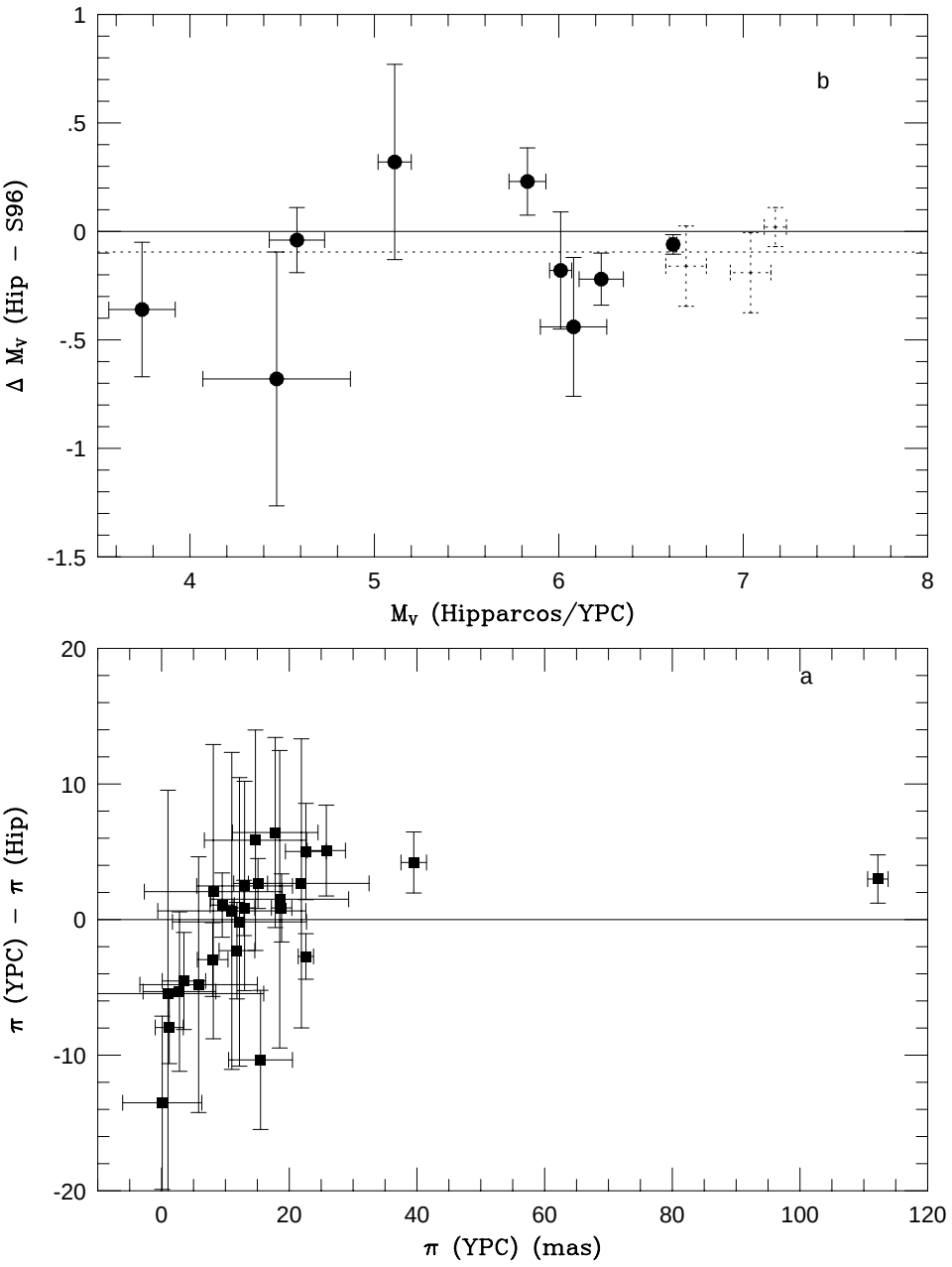

Fig. 2.— The lower panel shows a comparison between ground-based parallax measurements and Hipparcos astrometry for 26 stars in common between the current sample and the Yale Parallax catalogue. The upper panel compares the absolute magnitudes adopted by S96 for twelve of the stars used in their M5 distance determination against the Hipparcos data (solid dots) and the final YPC data (triangles).

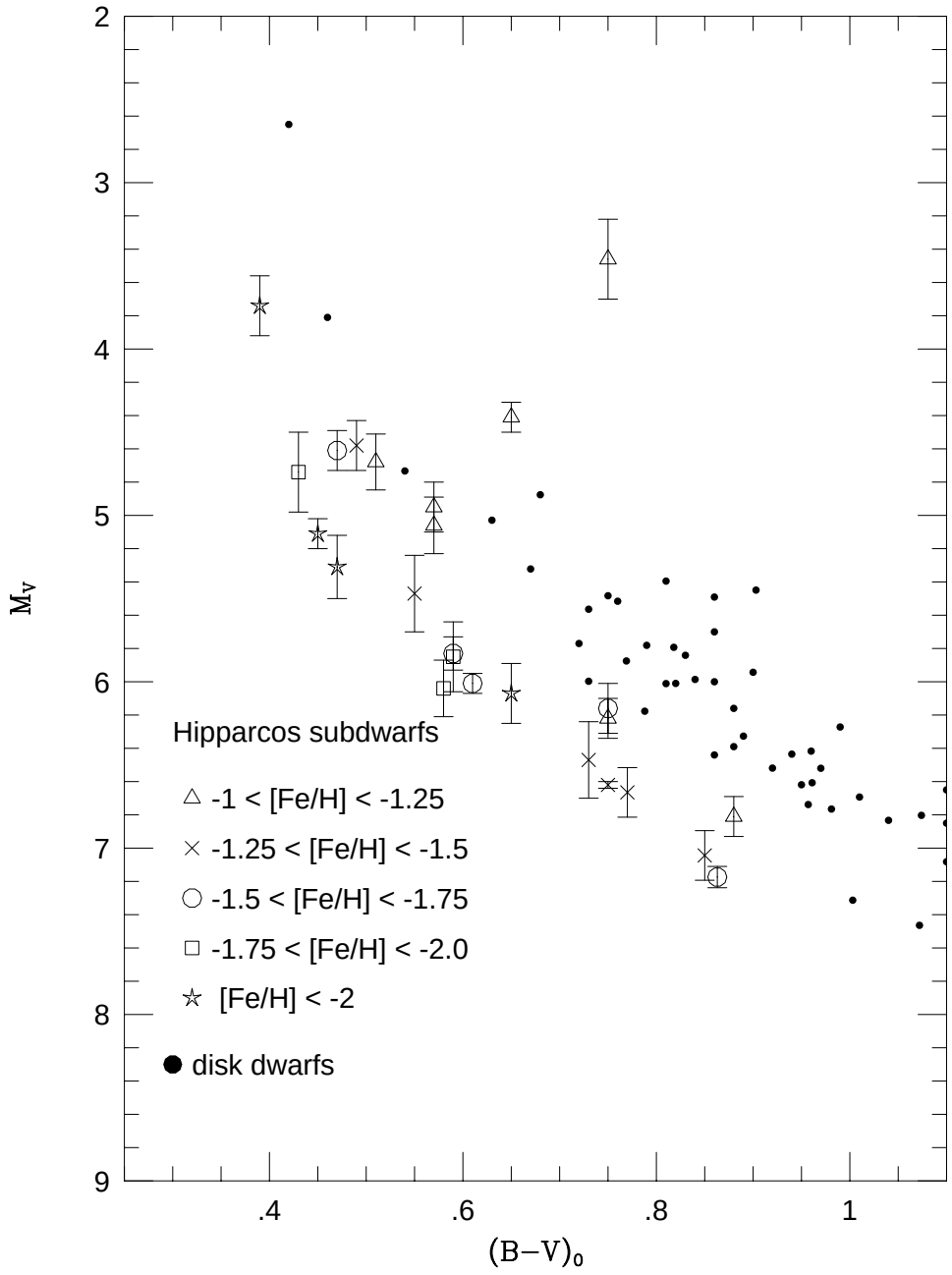

Fig. 3.— The main-sequence for metal-poor stars, defined by Lowell proper motion stars with measured abundances and Hipparcos parallaxes with precision of at least 12 %

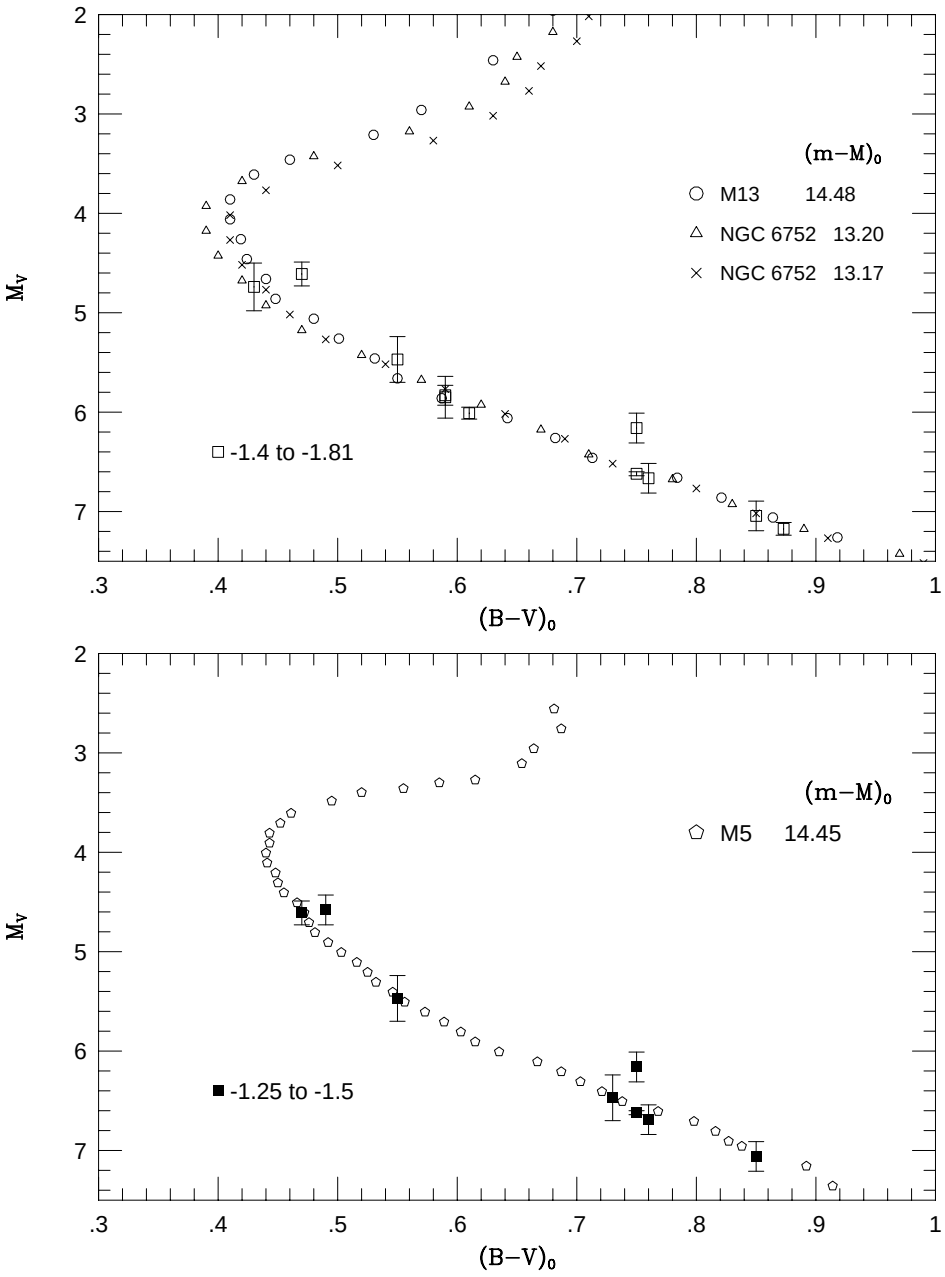

Fig. 4.— Main-sequence fitting for the three intermediate-abundance globular clusters discussed in this paper. The calibrating subdwarfs from the appropriate abundance range are plotted at the appropriate Lutz-Kelker corrected absolute magnitudes, and the errorbars indicate 1σ uncertainties.

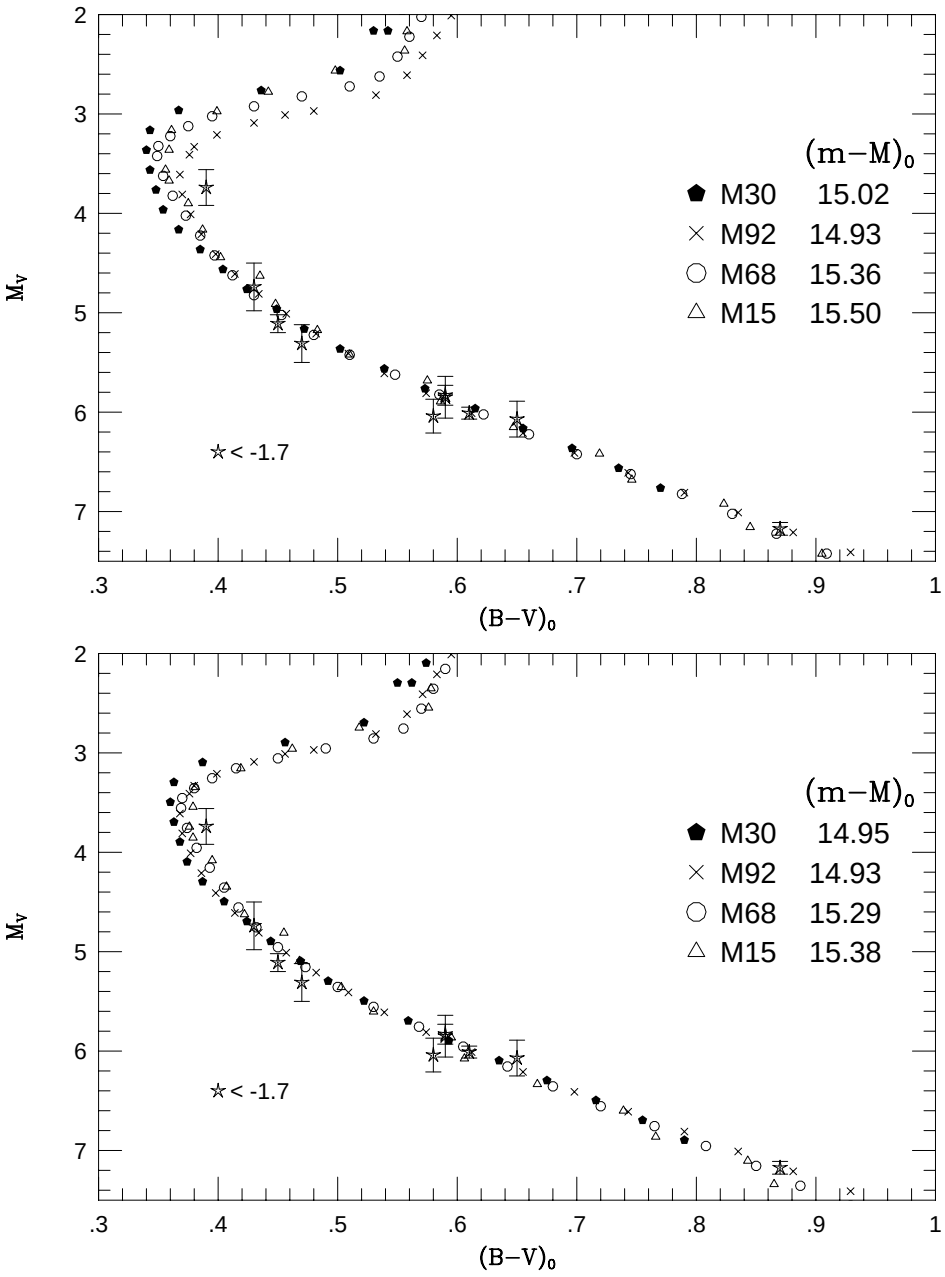

Fig. 5.— Main-sequence fitting for the four metal-poor globular clusters. Again, the relevant set of calibrating subdwarfs is shown. The reddening toward M15, M30 and M68 is not unambiguously determined, so we plot the results for two values of the extinction for those clusters. The upper panel shows the best-fit calibration for the highest reddenings listed in Table 3.

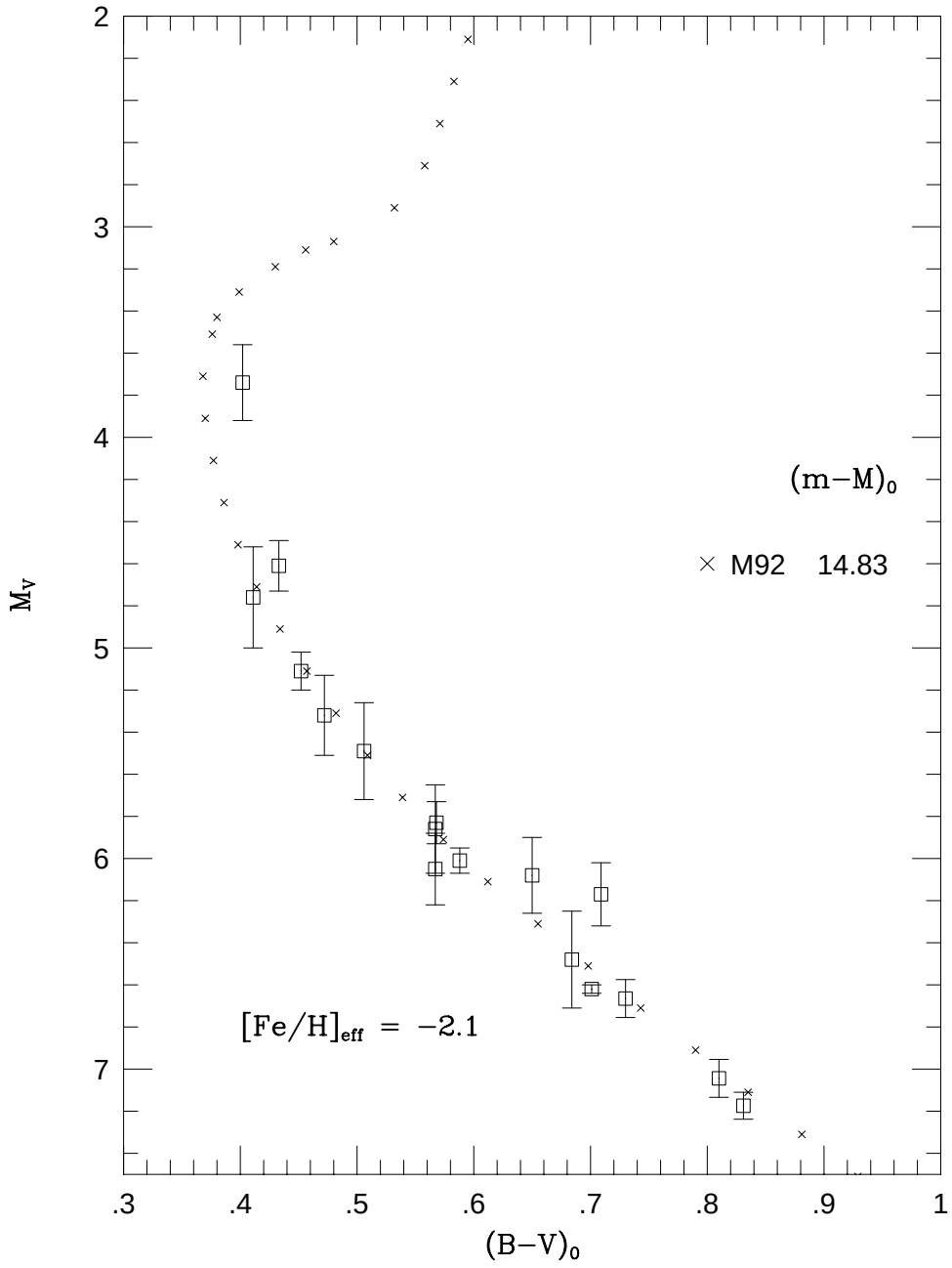

Fig. 6.— The results of matching the M92 fiducial sequence to an [Fe/H]=-2.1 monometallicity subdwarf sequence, using the Hipparcos stars as reference and with the differential colour corrections taken from the BV92 models

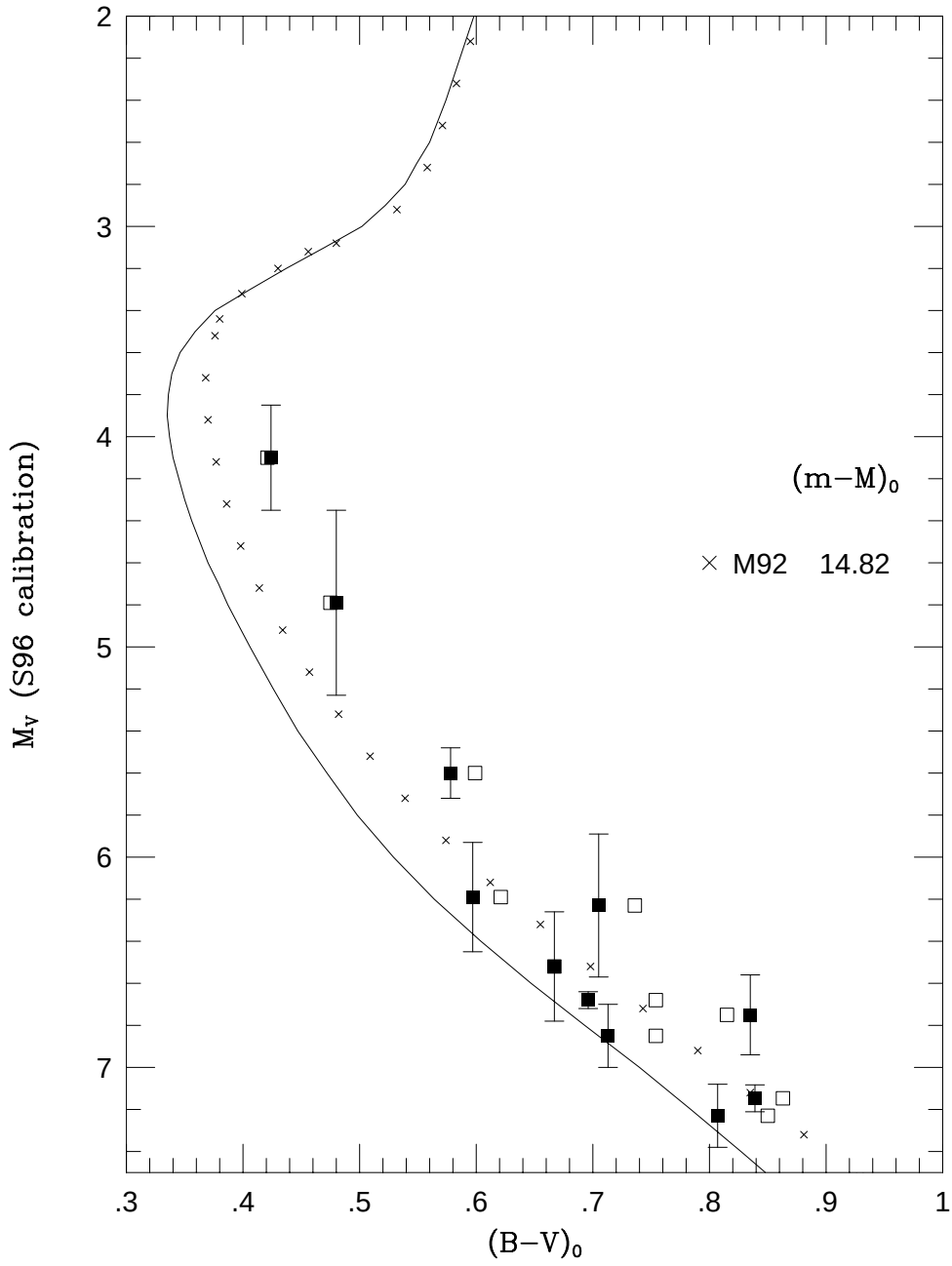

Fig. 7.— Main-sequence fitting for M92 using a subset of the S96 subdwarfs as the local calibrators. The open squares mark the observed positions of those stars *at the Lutz-Kelker corrected absolute magnitudes derived by S96*. The solid points mark the same stars after adjusting the (B-V) colours to match an [Fe/H]=-2.1 isophote. The calibrated M92 fiducial sequence is plotted together with the BV92 [Fe/H]=-2.26 14 Gyr isochrone.

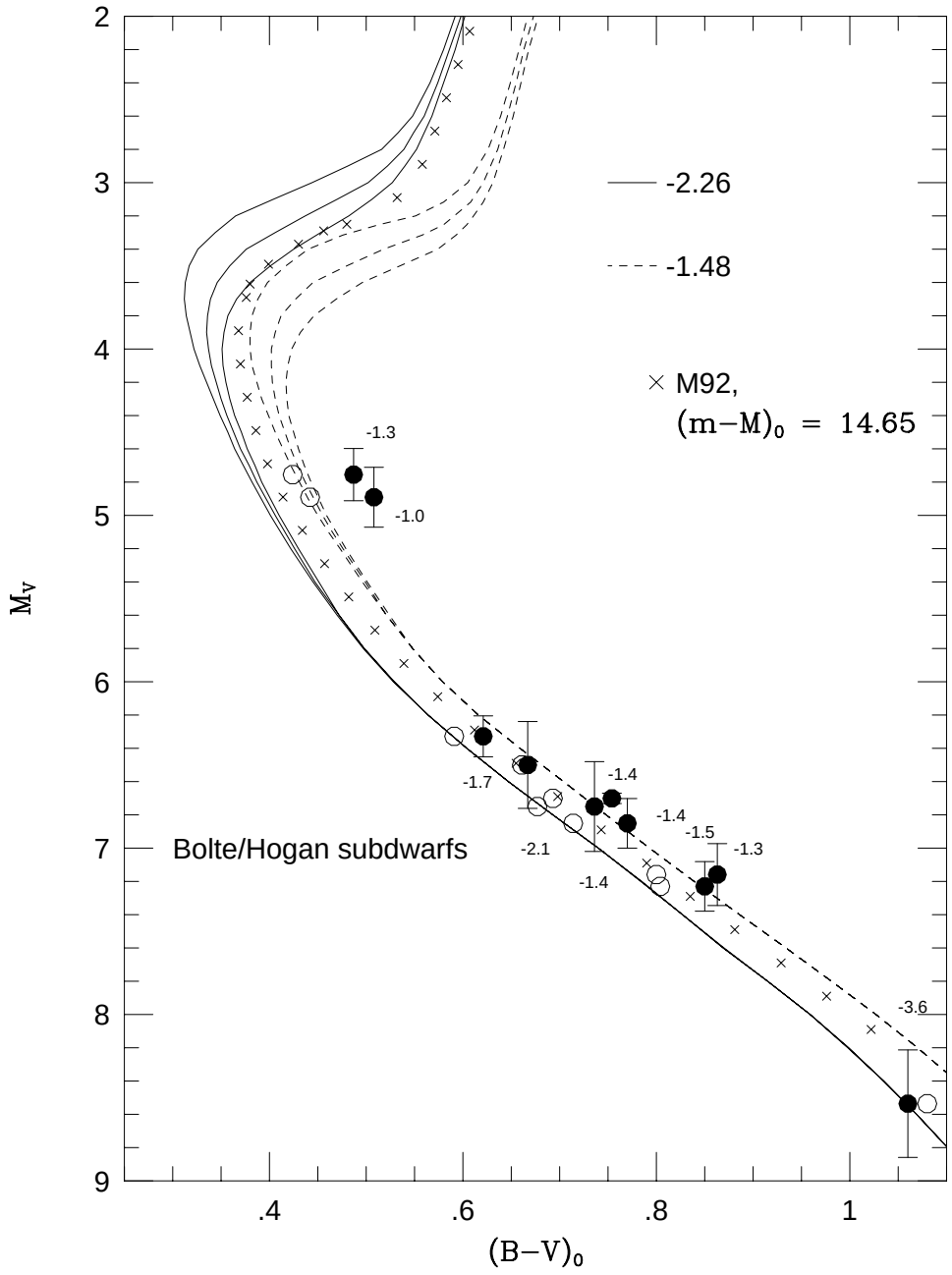

Fig. 8.— A comparison in the (M_V, (B-V)) plane between the BV92 oxygen-enhanced isochrones and the location of the ten subdwarf calibrators available to Bolte & Hogan (1995). The solid points mark the actual colours and magnitudes while the open circles show positions after adjusting to [Fe/H]=-2.26. The three isochrones plotted for each abundance are for ages of 12, 14 and 16 Gyrs.

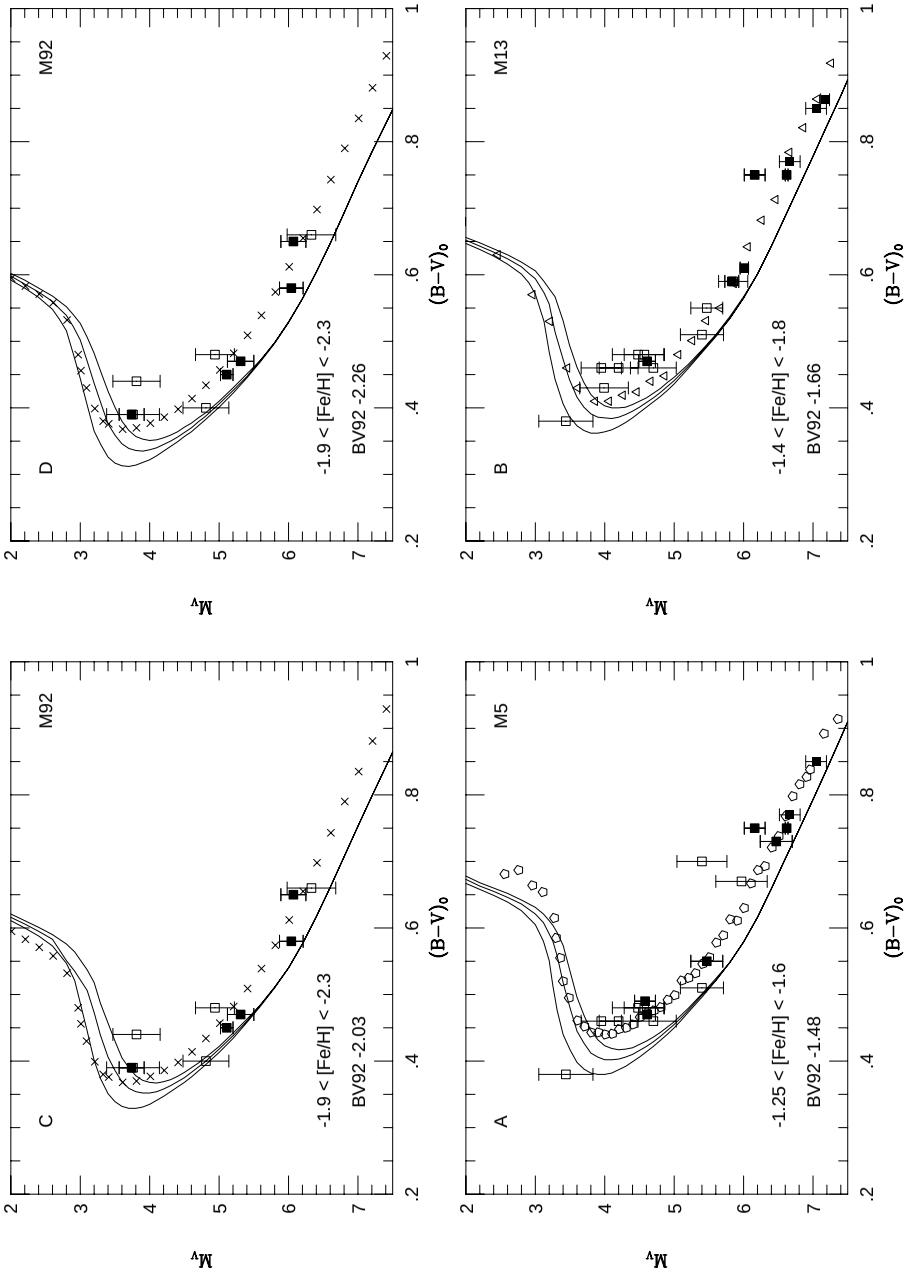

Fig. 9.— A comparison between the BV92 theoretical isochrones and the empirical main-sequence (M_V, (B-V)) defined by the local subdwarfs. Each sub-panel plots 12, 14 and 16 Gyr isochrones for a given abundance, together with the subdwarfs within the specified abundance range and the appropriate globular cluster fiducial sequence. Note that the cluster data are matched to the subdwarfs, not the isochrones.

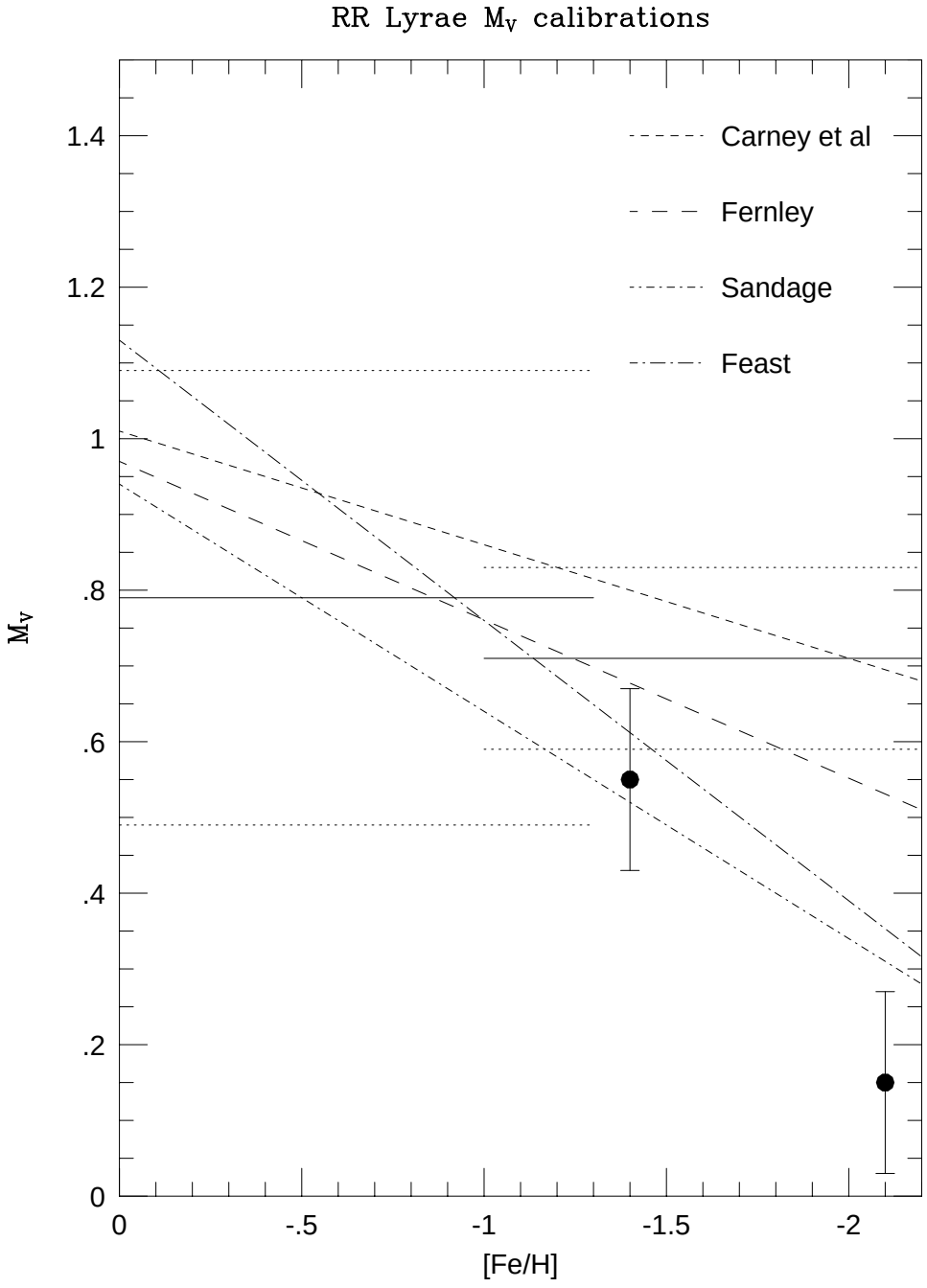

Fig. 10.— A comparison between the absolute magnitudes we derive for intermediate and extreme metal-poor RR Lyraes based on the distance moduli we derive respectively to M5 and the three clusters M92, M68 and M15. Previously derived (M_V, [Fe/H]) are also shown. The solid line marks the results derived by Layden et al from statistical parallax analysis of the local stars. The solid points mark our current results.

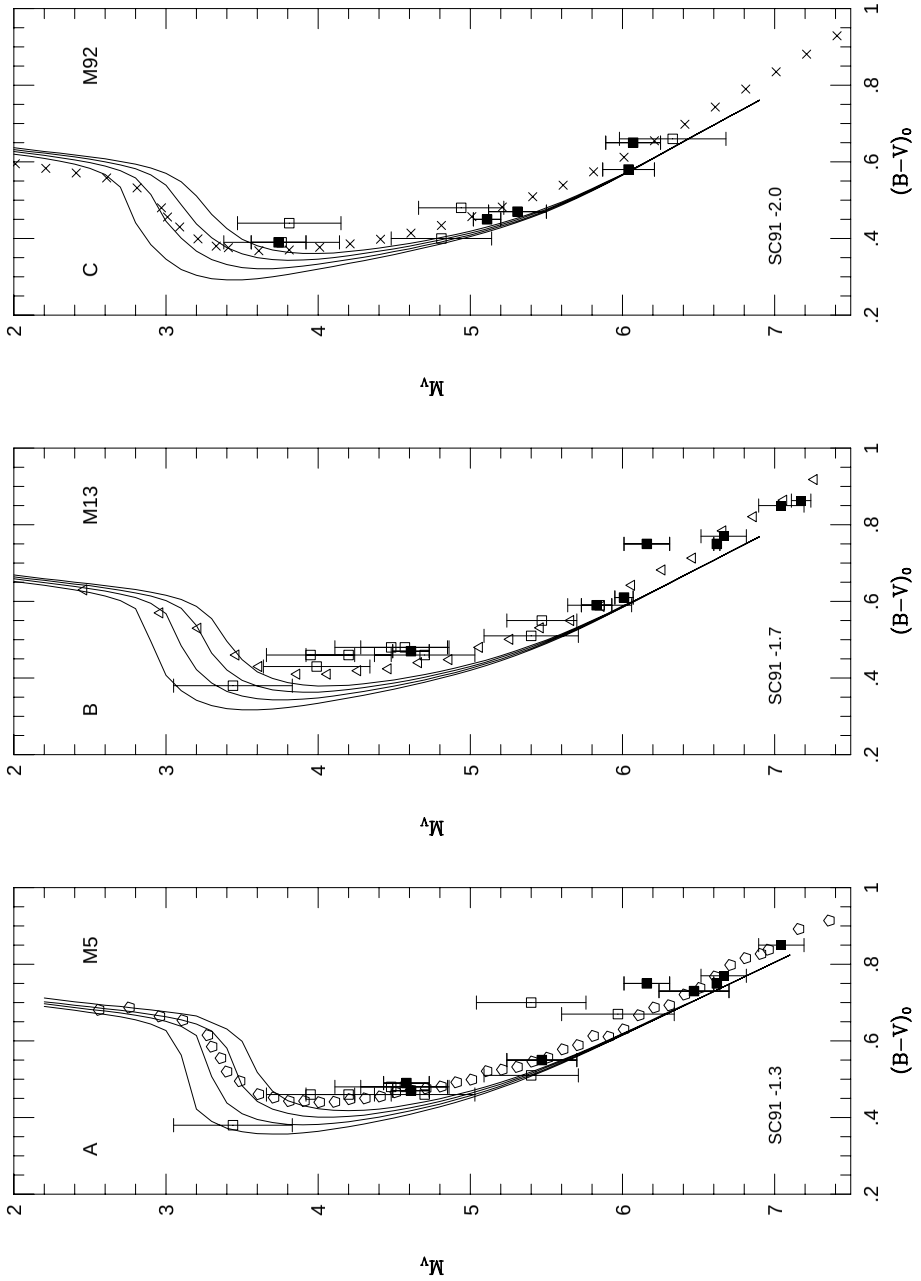

Fig. 11.— A comparison between the SC91 theoretical isochrones and the empirical main-sequence. As in figure 9, we show a set of model isochrones, for ages of 10, 12, 14 and 16 Gyrs and abundances of [Fe/H]=-1.3, -1.7 and -2.0.

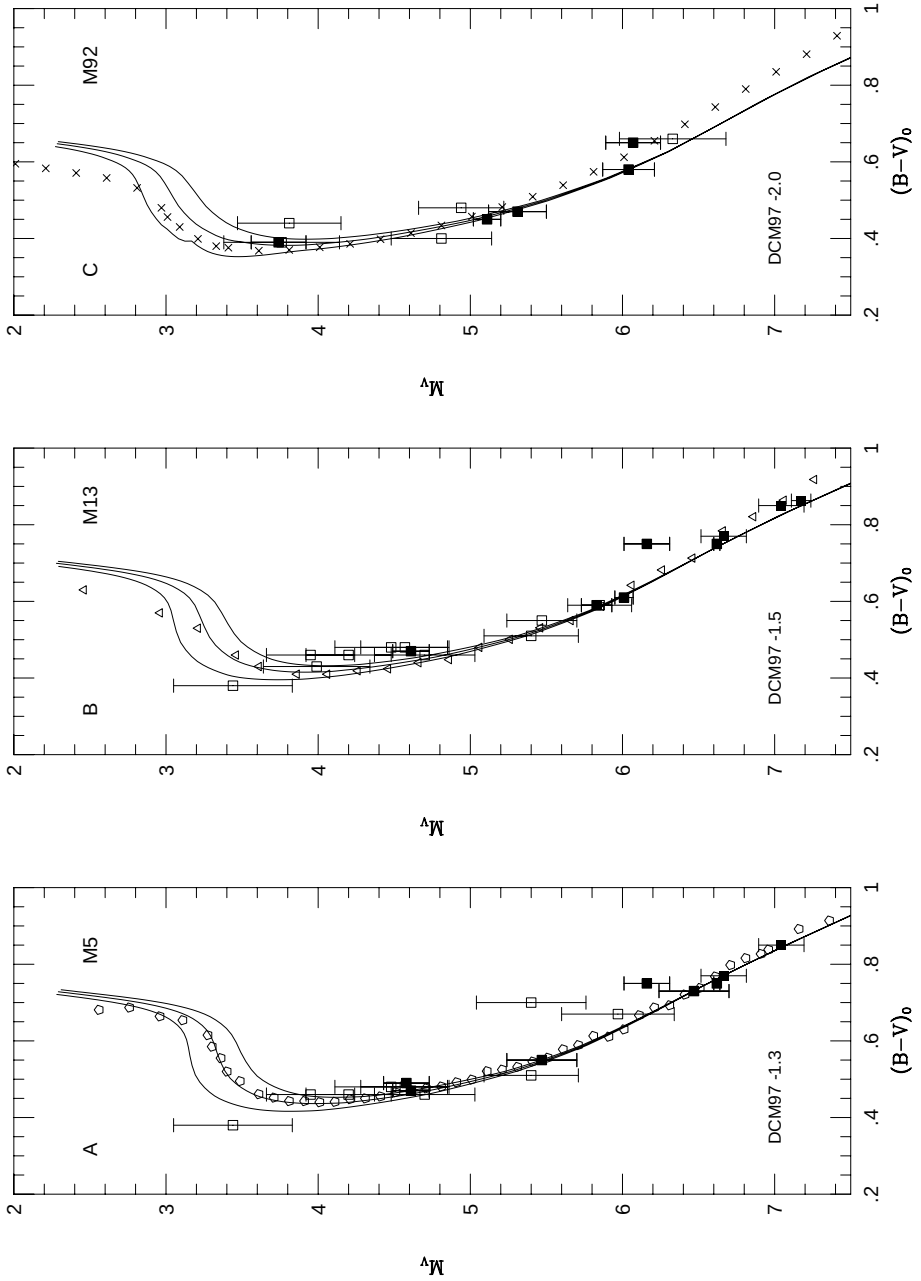

Fig. 12.— A comparison between the DCM theoretical isochrones and the empirical metal-poor main-sequence(s). The format is as in figures 9 and 11, with the theoretical isochrones plotted for ages of 10, 12 and 14 Gyrs and for abundances of [Fe/H] = -1.3, -1.5 and -2.0.

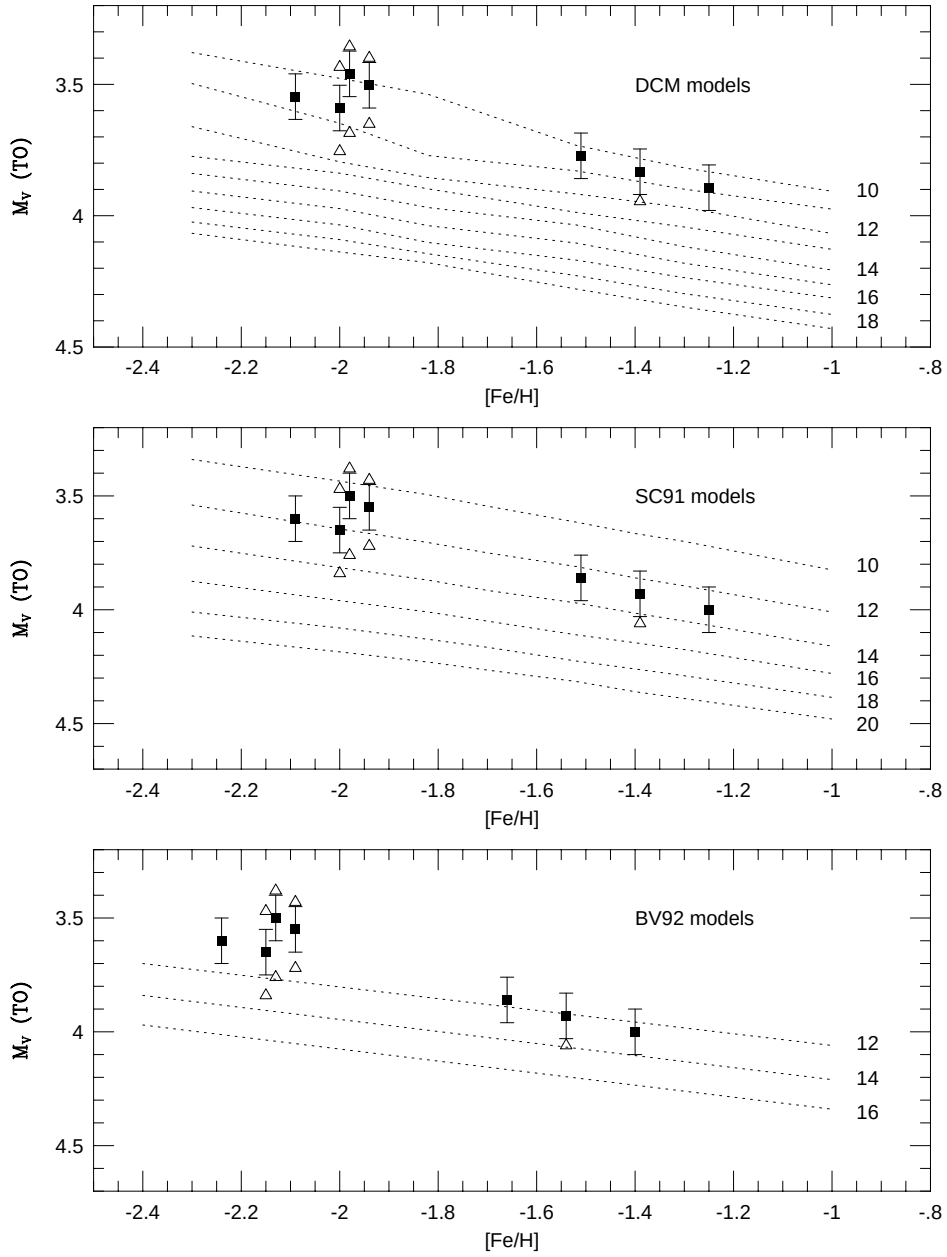

Fig. 13.— Age estimation using the luminosity of the main-sequence turnoff. The observed values of M_V(TO) are compared to the theoretical predictions of the SC91, BV92 and DCM models. The dotted lines show the predicted variation of M_V(TO) with abundance for a given age (listed on the right edge of each panel).

TABLE 1. The calibrating subdwarfs

Name		V_0	$(B-V)_0$	E_{B-V}	[Fe/H]	π (mas)	$\frac{\sigma_\pi}{\pi}$	M_V	M_V^{LK}	δ(B-V)
	$\frac{\sigma_\pi}{\pi} < 0.12$									
HD 19445	G37-26	8.06	0.45		-2.12	25.85	0.044	5.12	5.11	0.002
+66 268[1]	G246-38	9.91	0.65		-2.10	17.58	0.087	6.14	6.07	0.00
HD 64090[2]	G90-25	8.28	0.61		-1.75	35.29	0.030	6.02	6.01	-0.022
HD 84937[2]	G43-3	8.33	0.39		-2.18	12.44	0.085	3.80	3.74	0.012
HD 94028[2]	G58-25	8.22	0.47		-1.56	19.23	0.060	4.64	4.61	-0.037
+51 1696	G176-53	9.92	0.55		-1.44	13.61	0.113	5.59	5.47	-0.044
HD 103095	G122-51	6.43	0.75		-1.44	109.21	0.007	6.62	6.62	-0.049
HD 108177	G13-35	9.67	0.43		-1.81	10.95	0.118	4.87	4.74	-0.018
HD 149414[3]	G17-25	9.63	0.75		-1.54	20.71	0.072	6.21	6.16	-0.041
+5 3640	G140-46	10.43	0.73		-1.36	17.00	0.112	6.58	6.47	-0.046
HD 188510	G143-17	8.83	0.59		-1.75	25.32	0.046	5.85	5.83	-0.022
+42 3607	G125-64	9.99	0.47	0.04	-2.13	12.02	0.094	5.39	5.31	0.002
HD 194598	G24-15	8.35	0.49		-1.28	17.94	0.069	4.62	4.57	
+41 3931	G 212-7	10.18	0.59	0.03	-1.78	14.24	0.103	5.95	5.85	-0.024
+59 2407	G 231-52	10.19	0.58	0.05	-1.91	15.20	0.080	6.10	6.04	-0.013
	YPC data									
HD 25329		8.51	0.87		-1.73	54.3	0.026	7.18	7.17	-0.029
HD 134439		9.09	0.76		-1.57	33.5	0.051	6.72	6.69	-0.040
HD 134440		9.46	0.85		-1.52	33.5	0.051	7.09	7.06	-0.040
	$0.12 < \frac{\sigma_\pi}{\pi} < 0.2$									
HD 3567	G270-23	9.25	0.46		-1.50	9.57	0.144	4.15	3.95	
+71 31	G242-65	10.23	0.39		-2.27	6.04	0.189	4.14	3.76	
+72 94[2]	G245-32	9.80	0.38	0.04	-1.62	6.46	0.197	3.85	3.44	
+54 1216	G194-22	9.69	0.48		-1.64	10.36	0.142	4.77	4.57	
-3 2525[2]	G114-26	9.66	0.48		-1.90	12.37	0.139	5.12	4.94	
+36 2165	G119-64	9.76	0.43		-1.75	8.11	0.176	4.31	3.99	
	G254-24	11.53	0.66		-2.26	10.52	0.174	6.64	6.33	
HD 106038	G12-21	10.16	0.46		-1.45	9.16	0.164	4.97	4.70	
+1 2831[3]	G62-52	10.89	0.67		-1.33	12.26	0.186	6.33	5.97	
+6 2932[1]	G66-22	10.46	0.70		-1.30	11.38	0.181	5.74	5.40	
+26 2606[3]	G166-45	9.72	0.43		-2.58	10.28	0.138	4.78	4.60	
+42 2667	G180-24	9.86	0.46		-1.53	8.03	0.139	4.38	4.20	
+2 3375	G20-8	9.92	0.44	0.01	-2.55	8.35	0.196	4.53	4.12	
+36 2964	G182-31	10.34	0.41	0.01	-2.53	5.91	0.198	4.20	3.78	
+26 4136[1]	G 187-40	10.45	0.51	0.02	-1.55	10.90	0.156	5.64	5.40	
+26 4251	G188-22	10.02	0.48	0.01	-1.45	9.19	0.185	4.84	4.48	
LHS 3731	G188-30	11.00	0.64	0.01	-1.86	10.60	0.196	6.13	5.71	
+17 4708[3]	G126-62	9.47	0.44		-1.95	8.43	0.168	4.10	3.81	
+38 4955[3]	G190-15	11.01	0.65	0.01	-2.68	14.09	0.156	6.75	6.51	
+59 2723[3]	G217-8	10.34	0.40	0.05	-2.24	8.85	0.162	5.07	4.81	

[1]Suspected as non-single from Hipparcos analysis
[2]Suspected single-lined binary, CLLA
[3]Confirmed single-lined binary, CLLA

TABLE 2. The cluster sample - reddening

Cluster	E_{B-V} BH	E_{B-V} Z80	E_{B-V}	ref	E_{B-V}	ref
M 5	0.03	0.03	0.02	1		
NGC 6752	0.04	0.00	0.02-0.05	2		
M 13	0.02	0.01				
M 68	0.07	0.02	0.07±0.01	3	0.03	4
M 30	0.02	0.01	0.068±0.035	5		
M 15	0.08	0.08	0.10±0.02	6	0.11±0.04	7
M 92	0.02	0.03				

Notes to Table 2.

column 1 : reddening from Burstein & Heiles (1982)
column 2 : reddening from Zinn (1980)
Other references for reddening :
1. from data of Reid, 1996 : blue edge of instability strip (IS)
2. Carney, 1979 : UBV & DDO photometry of HB stars and field stars
3. Walker, 1994 : red, blue edge of IS; Sturch RR Lyr; (V-I) of RGB
4. Brocato et al, 1994 : blue edge of IS, pulsational theory
5. Richer et al, 1988 : UBV for BHB stars
6. Bingham et al, 1984 : Sturch RR Lyr, HB photometry
7. Richer & Fahlman, 1986 : UBV for field stars

TABLE 3. The cluster sample - distance estimates

Cluster	E_{B-V}	$[Fe/H]_{ZW}$	$[Fe/H]_{CG}$	$(m-M)_{old}$	ref.	$(m-M)_{12}$	$(m-M)_{20}$	$(m-M)_{-2.1}$
M 5	0.03	-1.4	-1.11	14.32	1	14.45	14.50	
NGC 6752	0.04	-1.54	-1.42	13.23	2	13.20	13.25	
	0.02			13.23	2	13.17	13.20	
M 13	0.02	-1.65	-1.39	14.44	3	14.48	14.55	
M 68	0.07	-2.09	-1.99	15.04	4	15.37	15.47	15.27
	0.05				4	15.29	15.37	15.20
	0.03				4	15.19	15.25	15.13
M 30	0.07	-2.13	-1.91	14.64	5	15.01	15.11	14.92
	0.05				5	14.95	15.05	14.86
	0.02				5	14.78	14.87	14.75
M 15	0.11	-2.15	-2.12	15.09	6	15.51	15.58	15.36
	0.09				6	15.38	15.39	15.27
	0.07				6	15.25	15.33	15.22
M 92	0.02	-2.24	-2.16	14.65	7	14.93	15.02	14.83

Notes to Table 3.

References for reddening & previous distance moduli $(m-M)_{old}$:
1. Sandquist et al, 1996
2. Penny & Dickens, 1985
3. Richer & Fahlman, 1986
4. McClure et al, 1987
5. Richer, Fahlman & Vandenberg, 1986
6. Durrell & Harris, 1993
7. Bolte & Hogan, 1995

All of the distances listed are true distance moduli.